

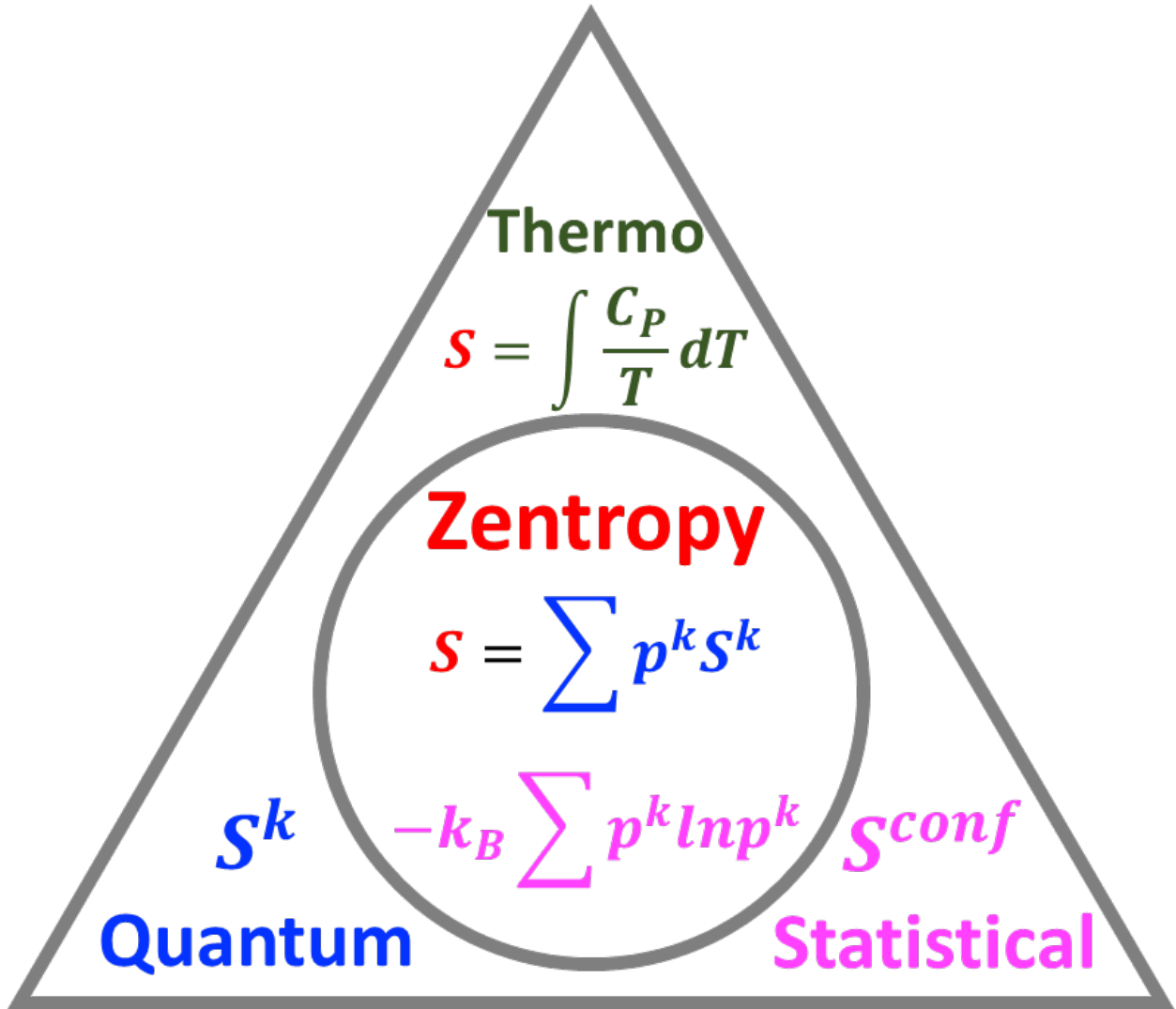
# Quantitative Predictive Theories through Integrating Quantum, Statistical, and Equilibrium, and Nonequilibrium Thermodynamics

Zi-Kui Liu

Department of Materials Science and Engineering, The Pennsylvania State University,  
University Park, Pennsylvania 16802, USA

## Abstract:

Today's thermodynamics is largely based on the combined law for equilibrium systems and statistical mechanics derived by Gibbs in 1873 and 1901, respectively, while irreversible thermodynamics for nonequilibrium systems resides essentially on the Onsager Theorem as a separate branch of thermodynamics developed in 1930s. Between them, quantum mechanics was invented and was quantitatively solved in terms of density functional theory (DFT) in 1960s. These three scientific domains operate based on different principles and are very much separated from each other. In analogy to the parable of the blind men and the elephant articulated by Perdue, they individually represent different portions of a complex system and thus are incomplete by themselves alone, resulting in the lack of quantitative agreement between their predictions and experimental observations. Over the last two decades, the author's group has developed a multiscale entropy approach (recently termed as zentropy theory) that integrates DFT-based quantum mechanics and Gibbs statistical mechanics and is capable of accurately predicting entropy and free energy of complex systems. Furthermore, in combination with the combined law for nonequilibrium systems developed by Hillert, the author developed the theory of cross phenomena beyond the phenomenological Onsager Theorem. The zentropy theory and theory of cross phenomena jointly provide quantitative predictive theories for experimental observables as reviewed in the present work.



Schematic representation of the zentropy theory for the total entropy  $S$  with contributions from each configuration  $k$  via DFT-based calculations ( $S^k$ ) and configurational entropy ( $S^{conf} = -k_B \sum p^k \ln p^k$ ) among configurations with the probability  $p^k$  for each configuration  $k$ , which is equal to the entropy from the integration of experimental heat capacity ( $C_P$ ).

# Table of Contents

<b>1</b>	<b>INTRODUCTION.....</b>	<b>5</b>
<b>2</b>	<b>GIBBS EQUILIBRIUM THERMODYNAMICS, DFT-BASED QUANTUM MECHANICS, AND STATISTICAL MECHANICS.....</b>	<b>8</b>
2.1	GIBBS EQUILIBRIUM THERMODYNAMICS.....	8
2.2	DFT-BASED QUANTUM MECHANICS .....	11
2.3	STATISTICAL MECHANICS .....	14
<b>3</b>	<b>HILLERT NONEQUILIBRIUM THERMODYNAMICS, ONSAGER THEOREM, PRIGOGINE ENTROPY BALANCE, AND AGREN ATOMIC MOBILITY .....</b>	<b>16</b>
3.1	HILLERT NONEQUILIBRIUM THERMODYNAMICS.....	16
3.2	ONSAGER THEOREM .....	20
3.3	PRIGOGINE ENTROPY BALANCE .....	22
3.4	AGREN ATOMIC MOBILITY .....	24
<b>4</b>	<b>ZENTROPY THEORY.....</b>	<b>27</b>
4.1	MULTISCALE ENTROPY AND ITS COARSE-GRAINING.....	27
4.2	STATISTICAL MECHANICS BASED ON THE ZENTROPY THEORY .....	28
4.3	PREDICTION OF EMERGENT BEHAVIORS IN MAGNETIC MATERIALS BY ZENTROPY THEORY.....	30
4.3.1	<i>General discussion of emergent behaviors.....</i>	<i>30</i>
4.3.2	<i>Emergent behaviors in magnetic materials.....</i>	<i>33</i>
4.3.3	<i>On <math>YNiO_3</math> with strongly correlated physics.....</i>	<i>36</i>
4.3.4	<i>Miscalculation of entropy on “microscopic violation of second law of thermodynamics” .....</i>	<i>38</i>
<b>5</b>	<b>THEORY OF CROSS PHENOMENA .....</b>	<b>39</b>
5.1	ISSUES ON ONSAGER THEOREM AND PRIGOGINE ENTROPY BALANCE.....	39
5.2	FORMULATION OF INTERNAL PROCESSES AND ENTROPY PRODUCTION .....	42

5.3	FORMULATION OF THEORY OF CROSS-PHENOMENA.....	45
5.4	APPLICATIONS OF THEORY OF CROSS PHENOMENA.....	46
5.4.1	<i>Thermoelectricity</i> .....	47
5.4.2	<i>Thermodiffusion</i> .....	50
5.4.3	<i>Electromigration</i> .....	52
5.4.4	<i>Electrocaloric effect</i> .....	53
5.4.5	<i>Electromechanical effect</i> .....	55
<b>6</b>	<b>SUMMARY AND OUTLOOKS.....</b>	<b>56</b>
<b>7</b>	<b>ACKNOWLEDGEMENTS.....</b>	<b>59</b>
<b>8</b>	<b>REFERENCES.....</b>	<b>60</b>

## 1 Introduction

As written in the preface of “The collected works of J. Willard Gibbs: Vol. I Thermodynamics”<sup>1</sup>, Gibbs spent the winter of 1866-67 in Paris and the following year in Berlin where he heard the lectures of Magnus and other teachers of physics and mathematics. In 1868 he went to Heidelberg, where Kirchhoff and Helmholtz were then stationed, before returning to the US in June, 1869. In 1873, Gibbs<sup>2</sup> introduced entropy change into the 1<sup>st</sup> law of thermodynamics using the relation between entropy change and heat change by Clausius for an reversible process of a closed system under hydrostatic pressure and extended it to multicomponent system in 1875/1876 and 1877/1878<sup>3,4</sup>. In searching for description of absolute entropy, Gibbs<sup>5</sup> took a broader view of statistical mechanics based on the foundation established by Clausius, Maxwell, and Boltzmann and “imagined a great number of systems of the same nature, but differing in the configurations and velocities which they have at a given instant, and differing not merely infinitesimally, but it may be so as to embrace every conceivable combination of configuration and velocities” in 1901. This resulted in the configurational entropy in terms of the probabilities of the configurations and the statistical mechanics commonly used today. While Gibbs principally focused on thermodynamic and statistical equilibrium in his work, but did mention free energy change for nonequilibrium systems<sup>3,4</sup>.

In contrast to the macroscopic top-down view of systems by Gibbs, quantum mechanics developed in 1920s examines the interactions among electrons and atoms and considers a condensed matter as a collection of interactions among positively charged nuclei and negatively charged electrons. Theoretically these interactions can be treated by solving the many-body Schrödinger equation involving both the nuclei and the electrons<sup>6</sup>. The Gibbs classic statistical

mechanics was also updated to quantum statistical mechanics <sup>7</sup>. The solutions to the many-body nature of the interactions in quantum mechanics were developed in 1960's in terms of the density functional theory (DFT) that aims to represent the outcome of those interactions and articulates that for a given system, there exists a ground-state configuration at 0 K that its energy is at its minimum value with a universal functional of the interacting electron gas density <sup>8</sup>. This unique ground-state electron density is obtained by explicitly separating the independent-electron kinetic energy and long-range Coulomb interaction energy and replacing the many-body electron problem using independent valence electrons with an exchange-correlation functional of the electron density and an associated exchange-correlation energy <sup>9</sup>.

In last 60 years, significant processes have been made in developing the exchange-correlation functionals, particularly the generalized gradient approximation (GGA) <sup>10-12</sup>, in which the exchange-correlation energy is treated as a function of both the local electron density and its gradient. The latest meta-GGA includes the strongly constrained and appropriately normed (SCAN) <sup>13,14</sup> and  $r^2$ SCAN with both improved accuracy and numerical stability and efficiency <sup>14-19</sup>. For property of the ground-state configurations at finite temperature, the entropy of thermal electrons can be formulated <sup>9</sup> through the generalization of ground-state energy of an interacting inhomogeneous electron gas by Mermin <sup>20</sup>, and the entropy of phonons through the lattice vibrations <sup>21</sup>.

Since the 2<sup>nd</sup> law of thermodynamics was effectively excluded in the Gibbs thermodynamics due to its inequality, this resulted in the development of irreversible thermodynamics phenomenologically <sup>22</sup> based on experimental observations rather than from the 1<sup>st</sup> and 2<sup>nd</sup> laws

of thermodynamics<sup>23</sup>. They are represented by the Onsager theorem<sup>24,25</sup> followed by the unified formulation of dynamics and thermodynamics by Prigogine et al.<sup>26-31</sup>. Onsager<sup>24</sup> himself noted that “the principle of microscopic reversibility is less general than the fundamental laws of thermodynamics”, which is actually incompatible with irreversible internal processes<sup>32,33</sup>.

About two decades ago, the author’s group started to explore quantitative approaches in efforts to accurately predict the temperature-pressure (T-P) phase diagram without fitting parameters through integration of DFT and statistical mechanics, using the magnetic transitions in Ce as the first example with two<sup>34</sup> and three<sup>35</sup> configurations, respectively. By considering the entropy contributions from DFT-based calculations in terms of electrons and phonons and the configurational entropy among the ground-state and non-ground-state configurations to the total entropy, the T-P and T-V phase diagrams of Ce were accurately predicted without fitting parameters. This multi-scale entropy approach<sup>36</sup> was recently termed as the zentropy theory<sup>37</sup> and has been successfully used to accurately predict magnetic phase transition temperatures and property anomalies in a number of magnetic materials<sup>38</sup>, including the negative thermal expansion in Fe<sub>3</sub>Pt<sup>39</sup> and strongly correlated physics in YNiO<sub>3</sub><sup>40,41</sup>.

With the accurate prediction of free energy using the zentropy theory and inspired by the collaboration on thermodiffusion with Murch and his team<sup>42-46</sup>, the author<sup>32</sup> revisited the irreversible thermodynamics from the combined 1<sup>st</sup> and 2<sup>nd</sup> law of thermodynamics with internal processes emphasized by Hillert<sup>22</sup>. By examining the fundamental flaws of the Onsager theorem and considering the correlations between flux equations as internal processes in a system, the author presented a theory of cross phenomena based on combined 1<sup>st</sup> and 2<sup>nd</sup> law of

thermodynamics that captures the experimental observations that the Onsager theorem aimed to phenomenologically represent and enables the prediction of cross phenomena coefficients as 2<sup>nd</sup> derivatives of free energy <sup>32,33</sup>.

In this overview paper, the zentropy theory and theory of cross phenomena will be presented along with potential improvements and future applications. The rest of the paper is organized as follows: Section 2 for overview of Gibbs equilibrium thermodynamics, DFT-based quantum mechanics, and statistical mechanics; Section 3 for Hillert nonequilibrium thermodynamics, Onsager theorem, Prigogine entropy balance, and Agren atomic mobility; Section 4 for the zentropy theory; Section 5 for the theory of cross phenomena; and Section 6 for summary and future outlooks.

## **2 Gibbs equilibrium thermodynamics, DFT-based quantum mechanics, and statistical mechanics**

### **2.1 Gibbs equilibrium thermodynamics**

Employing the relation between entropy change and heat change by Clausius for an reversible process of a closed system under hydrostatic pressure, Gibbs <sup>2</sup> replaced the heat change in the 1<sup>st</sup> law of thermodynamics by the entropy change and obtained the combined law of thermodynamics for a closed *equilibrium* system, which is written in today's convention as follows

$$dU = dQ + dW = TdS - PdV \quad \text{Eq. 1}$$

where  $dU$  is the internal energy change of the system,  $dQ$ ,  $dW$ ,  $dS$  and  $dV$  are the increases of heat, work, entropy, and volume of the system controlled from the surroundings, and  $T$  and  $P$  are



the temperature and pressure. It is important to realize that even though Eq. 1 is commonly referred to as the combined 1<sup>st</sup> and 2<sup>nd</sup> law of thermodynamics or simply combined law of thermodynamics, it does not contain the key concept of the 2<sup>nd</sup> law of thermodynamics, i.e., the positive entropy production due to irreversible internal processes (*ip*) represented by the following equation

$$d_{ip}S > 0 \qquad \text{Eq. 2}$$

It is thus evident that Eq. 1 is valid only for  $d_{ip}S \leq 0$ , i.e., equilibrium systems without any possible internal processes by itself.

In a subsequent paper in the same year, Gibbs<sup>47</sup> emphasized that the relation between U, S, and V carries more knowledge than the other combinations of quantities in Eq. 1 such as V, P and T proposed by Thomson in 1871. Gibbs<sup>48</sup> termed Eq. 1 as the fundamental equation, representing the internal energy as a function of S and V, i.e., U(S,V), with S and V as the natural variables of U<sup>22</sup>. Gibbs<sup>47</sup> further articulated that at equilibrium T and P are both homogeneous in all phases of solid, liquid, and vapor. Gibbs' publications prompted Maxwell to make two three-dimensional models to represent the internal energy surface as a function of entropy and volume with one copy sent to Gibbs<sup>1</sup> and one kept in Cavendish Laboratory at the University of Cambridge<sup>33</sup>.

In his next long and more well-known publication in 1878, Gibbs<sup>48</sup> discussed the conditions of equilibrium for heterogeneous masses and introduced the concept of chemical potential with Eq. 1 revised as follows for a system with *c* independent components in today's convention

$$dU = TdS - PdV + \sum_{i=1}^c \mu_i dN_i = \sum_{a=1}^{c+2} Y^a dX^a \quad \text{Eq. 3}$$

where  $\mu_i$  is the chemical potential of component  $i$ ,  $N_i$  the moles of component  $i$ , and  $Y^a$  and  $X^a$  represent the pairs of conjugate variables with  $Y^a$  for potentials, such as  $T$ ,  $P$ , and  $\mu_i$ , and  $X^a$  for molar quantities, such as  $S$ ,  $V$ , and  $N_i$  <sup>22,33,49</sup>. As it will be shown later in this paper,  $\mu_i$  can be introduced in a way to better define its physical significance. It is noted that Gibbs called  $\mu_i$  potentials and considered pressure as a potential too when discussing equilibrium related to surfaces, which are generalized to include temperature plus stress, electric, and magnetic fields in general <sup>22,33,49</sup>.

Gibbs <sup>48</sup> elegantly demonstrated that every potential,  $Y^a$ , is homogeneous in the system with multiple phases in equilibrium with each other and further derived the integral form of Eq. 3 as follows for a homogeneous system

$$U = TS - PV + \sum_{i=1}^c \mu_i N_i = \sum_{a=1}^{c+2} Y^a X^a \quad \text{Eq. 4}$$

In the same paper, Gibbs <sup>48</sup> introduced the now-termed free energies such as Helmholtz energy ( $F = U - TS$ ), enthalpy ( $H = U + PV$ ), and Gibbs energy ( $G = U - TS + PV = \sum_{i=1}^c \mu_i N_i$ ) and re-wrote Eq. 3 accordingly, e.g., Gibbs energy as follows,

$$dG = -SdT + VdP + \sum_{i=1}^c \mu_i dN_i \quad \text{Eq. 5}$$

Gibbs <sup>48</sup> further presented the now-termed Gibbs-Duhem equation as follows

$$d\Phi = d(G - \sum_{i=1}^c \mu_i N_i) = -SdT + VdP - \sum_{i=1}^c N_i d\mu_i = 0 \quad \text{Eq. 6}$$

along with the now-termed Gibbs phase rule for an equilibrium with  $p$  co-existing phases and the now-termed Clausius-Clapeyron equation in terms of temperature and pressure between two phases in equilibrium

$$v = c + 2 - p \quad \text{Eq. 7}$$

$$\frac{dP}{dT} = \frac{\Delta S}{\Delta V} = \frac{\Delta H}{T\Delta V} \quad \text{Eq. 8}$$

where  $v$  represents the number of *independent potentials* for such an equilibrium, and  $\Delta S$ ,  $\Delta V$ , and  $\Delta H$  are the differences of entropy, volume, and enthalpy between the two phases. While Gibbs<sup>48</sup> did not explicitly discuss the entropy production due to internal processes, but demonstrated that  $dU > 0$ ,  $dG > 0$ , and  $d\Phi > 0$  for a stable equilibrium and further wrote

$$\frac{\partial Y^a}{\partial X^a} > 0 \quad \text{Eq. 9}$$

where all the other natural variables are kept constant. All partial derivatives in this present paper is written under such a convention unless a clarification is needed.

As the limit of stability is approached from the stable region of the system, one has  $\frac{\partial Y^a}{\partial X^a} = +0$  and  $\frac{\partial X^a}{\partial Y^a} = +\infty$ , i.e., the singularity or divergency of properties, and a critical point is reached with additionally  $\frac{\partial^2 Y^a}{\partial (X^a)^2} = 0$ . As will be shown later in this paper,  $d\Phi$  is directly related to entropy production due to internal processes in nonequilibrium systems, and the author suggested to name  $\Phi$  as *Duhem energy*<sup>33</sup>. As will be shown below, it may be better to name it as *Hillert energy*. Furthermore, Hillert<sup>22</sup> showed that the partial derivative by Eq. 9 with more potentials as natural variables is smaller than the one with more molar quantities as natural variables. When all other potentials are as natural variables, one obtains the Gibbs-Duhem equation as shown by Eq. 6.

## 2.2 DFT-based quantum mechanics

DFT represents the state-of-the-art solution of the multi-body Schrödinger equation with one equation for each valence electron in the system<sup>50</sup>. Its approximations include adiabatic or Born-Oppenheimer approximation for nuclei<sup>51</sup>; independent-electron approximation in an average effective potential collectively determined by the nuclei and all electrons with the exchange-correlation energy approximated as a local functional of the electron density in terms of the local spin density approximation (LSDA)<sup>52,53</sup> and GGA; and replacement of the strong Coulomb potential of the nucleus and the tightly bound core electrons by a pseudopotential as an effective potential acting on valence electrons such ultrasoft pseudopotentials and the projector augmented wave (PAW) method<sup>54</sup>.

The electron density is solved iteratively until the energy of the ground-state configuration converges at 0 K. Its Helmholtz energy at finite temperature includes the quasiharmonic contributions from thermal electrons and phonons as follows<sup>21</sup>

$$F = E^0 + F^{el} + F^{vib} = E - TS \quad \text{Eq. 10}$$

$$E = E^0 + E^{el} + E^{vib} \quad \text{Eq. 11}$$

$$S = S^{el} + S^{vib} \quad \text{Eq. 12}$$

where  $F$ ,  $E$ , and  $S$  are the Helmholtz energy, internal energy (the same as  $U$  commonly used in the combined law of thermodynamics), and entropy of the ground-state configuration,  $F^{el}$ ,  $E^{el}$ , and  $S^{el}$  the contributions of thermal electron to Helmholtz energy, internal energy, and entropy based on the Fermi–Dirac statistics for electrons, and  $F^{vib}$ ,  $E^{vib}$ , and  $S^{vib}$  the vibrational contributions to Helmholtz energy, internal energy, and entropy based on the Bose–Einstein statistics for phonons, respectively. The thermal electronic contributions can be obtained using the finite temperature generalization of ground-state energy of an interacting inhomogeneous

electron gas by Mermin<sup>20</sup> as shown by Kohn and Sham<sup>9</sup>. The vibrational contributions can be obtained by quasi-harmonic (QHA) phonon calculations or Debye model with the former being more accurate and the latter more efficient<sup>21,55</sup> through the high throughput DFT Tool Kits (DFTTK)<sup>56,57</sup>. The detailed equations for these quantities can be found in the literature<sup>21,49</sup>. For vibration-induced dipole-dipole long-range interactions, the author's group developed a mixed-space approach with the short-range interactions accounted for by supercells in the real space, the analytical solution for the origin in the reciprocal space which represents the infinite in the real space, and an interpolation scheme between them<sup>58-60</sup>.

An important development in the exchange-correlation energy approximation has emerged recently. In GGA<sup>10-12</sup> developed by Perdew and co-workers the exchange-correlation energy is treated as a function of both the local electron density and its gradient, resulting in more accurate predictions of electronic structure and the energy of ground-state configurations than LSDA. Over the years they and the community have developed various GGA functionals to improve the accuracy of DFT-based calculations. The latest SCAN meta-GGA<sup>13,14</sup> has significantly improved the quantitatively correct ground-state energetics by symmetry breaking for some systems regarded as strongly correlated<sup>17,19</sup>. The further developed  $r^2$ SCAN are with improved accuracy, numerical stability, and efficiency<sup>14-18</sup>. The key discovery in the SCAN meta-GGA is that "certain strong correlations present as fluctuations in the exact symmetry-unbroken ground-state wavefunction are 'frozen' in symmetry-broken electron densities or spin densities of approximate DFT"<sup>19</sup>. Consequently, an approximate density functional for exchange and correlation with symmetry breaking, though less accurate than an exact functional, is more revealing with its utility demonstrated for a number of cases<sup>17-19</sup>.

It seems plausible that those symmetry-broken electron densities may be sampled by phonon calculations of the ground-state configuration such as the negative thermal expansions predicted at low temperatures in ice and Si<sup>61</sup>. This symmetry-broken configurations are in a scale finer than the symmetry-broken configurations in the zentropy theory to be discussed in Section 4, with the latter derived from the internal degrees of freedom of the ground-state configuration. The typical internal degrees of freedom in condensed matter include magnetic pin polarization, electric dipole polarization, atomic short-range ordering, and various defects such as vacancy, dislocation, stacking fault, twin, grain boundary, voids, and other ones at even larger scale. These non-ground-state configurations can be created by systematically varying the internal degrees of freedom of the ground-state configuration of a system, and their Helmholtz energies can be predicted using Eq. 10 to Eq. 12 if they are metastable. For unstable non-ground-state configurations, there will be imaginary frequencies in their phonon dispersion curves, and their Helmholtz energies can thus not be directly predicted by means of phonon calculations. On the other hand, they only appear as transitory states at finite temperature with their properties predicted by the statistical mixtures of other stable and metastable configurations by the zentropy theory discussed in Section 4.

### **2.3 Statistical mechanics**

Statistical mechanics introduced by Gibbs<sup>5</sup> considers the probabilities of all conceivable *independent* configurations that a system embraces rather than the individual particles in the system. Consequently, each configuration is under the same constraints as the system. By using the combined law of thermodynamics in terms of the internal energy<sup>1</sup> and differentiating the

internal variables in the system and the external variables from the surroundings, Gibbs <sup>5</sup> was able to evaluate the entropy due to the distribution of various configuration in the system, but did not consider the entropy of each configuration itself.

In formulating statistical mechanics in the framework of quantum mechanics, Landau and Lifshitz <sup>7</sup> introduced the number of quantum states in terms of the energy interval in the order of magnitude to the mean fluctuation of energy of the system and showed the entropy of the system in terms of the tracer of each quantum state. In the limit of the classical theory, they obtained the entropy of a system as Gibbs did as follows

$$S = -k_B \sum_{k=1}^m p^k \ln p^k \quad \text{Eq. 13}$$

where  $m$  is the number of configurations,  $p^k$  the probability of configuration  $k$ , and  $k_B$  is added here to be consistent with the current convention. Consequently, for a system of canonical ensemble under constant NVT, the partition function of the system ( $Z$ ) in relation to the Helmholtz energy of the system ( $F$ ) and the partition function ( $Z^k$ ) and internal energy ( $E^k$ ) of each configuration are written as follows

$$Z = e^{-\frac{F}{k_B T}} = \sum_{k=1}^m Z^k = \sum_{k=1}^m e^{-\frac{E^k}{k_B T}} \quad \text{Eq. 14}$$

$$\begin{aligned} F &= -k_B T \ln Z + k_B T \left( \sum_{k=1}^m p^k \ln Z^k - \sum_{k=1}^m p^k \ln Z^k \right) \\ &= \sum_{k=1}^m p^k E^k + k_B T \sum_{k=1}^m p^k \ln p^k = \sum_{k=1}^m p^k E^k - TS \end{aligned} \quad \text{Eq. 15}$$

$$p^k = \frac{Z^k}{Z} = \frac{e^{-\frac{E^k}{k_B T}}}{Z} = e^{-\frac{E^k - F}{k_B T}} \quad \text{Eq. 16}$$

Let us consider a hypothetical system with only one configuration at low temperature, and Eq. 38 thus becomes

$$F = E^k \quad \text{Eq. 17}$$

Since  $F = E^k - TS^k$  by definition, Eq. 17 gives  $S^k = 0$  as  $T \neq 0$ , indicating that the configurations do not have any internal degrees of freedom, i.e., they are pure quantum configurations. In DFT developed after the quantum statistical mechanics <sup>7</sup>, the ground-state configuration is not a pure quantum configuration, and its entropy is calculated by Eq. 12. It is thus necessary to modify the formula of the partition function as discussed in Section 4 in terms of the zentropy theory.

### **3 Hillert nonequilibrium thermodynamics, Onsager theorem, Prigogine entropy balance, and Agren atomic mobility**

#### **3.1 Hillert nonequilibrium thermodynamics**

As mentioned in Section 2.1, Gibbs <sup>2</sup> used Clausius' definition of entropy exchange ( $d_Q S$ ) between a closed equilibrium system and its surroundings to derive Eq. 1. For an open system, the exchange of mass between the system and its surroundings brings both the exchange of internal energy and entropy. Furthermore, if there are irreversible internal processes take place inside the system, the resulted entropy production contributes to the total entropy change of the system. Consequently, the total entropy change of the system is written as follows <sup>22,33,49</sup>

$$dS = \frac{dQ}{T} + \sum_{i=1}^c S_i dN_i + d_{ip} S \quad \text{Eq. 18}$$

where  $S_i$  is the partial entropy of component  $i$  defined as



$$S_i = \left( \frac{\partial S}{\partial N_i} \right)_{dQ=0, d_{ip}S=0, N_{j \neq i}} \quad \text{Eq. 19}$$

The work exchange between the system and its surroundings does not enter Eq. 2 directly, but indirectly by affecting internal processes. It is important to note that the total entropy change contains the contributions from both exchanges between the system and its surroundings (first two terms in Eq. 18) and the internal processes (last term). Therefore,  $dS$  can be either positive or negative, which is not in contradiction with the 2<sup>nd</sup> law of thermodynamics as the 2<sup>nd</sup> law of thermodynamics concerns only the entropy production due to an independent internal process represented by Eq. 2.

Consequently, the combined law of thermodynamics with internal processes can be revised from Eq. 1 as follows<sup>22,33,49</sup>

$$dU = dQ + dW + \sum_{i=1}^c U_i dN_i = TdS + dW + \sum_{i=1}^c \mu_i dN_i - Td_{ip}S \quad \text{Eq. 20}$$

$$\mu_i = U_i - TS_i = \left( \frac{\partial U}{\partial N_i} \right)_{d_{ip}S=0, X^a \neq N_i} \quad \text{Eq. 21}$$

where  $dW$  represent all types of work including mechanical, electric, and magnetic work, and  $U_i$  is the partial internal energy of component  $i$  defined as follows<sup>38,49</sup>,

$$U_i = \left( \frac{\partial U}{\partial N_i} \right)_{dQ=0, dW=0, N_{j \neq i}} \quad \text{Eq. 22}$$

The concept of the chemical potential is thus naturally introduced by Eq. 21, and it contains the contributions from both partial internal energy and partial entropy of the component<sup>38,49</sup>. The constraint of constant entropy production in Eq. 21 requires the heat exchange between the

system and its surroundings, signifying its difference from Eq. 22 which is for an adiabatic system even though both are for the change of internal energy with respect to the change of the amount of the component  $i$ .

The explicit inclusion of  $Td_{ip}S$  in the combined law of thermodynamics was emphasized by Hillert<sup>22</sup>. To differentiate Gibbs equilibrium thermodynamics, i.e., Eq. 3, the author proposes to name Eq. 20 “*Hillert nonequilibrium thermodynamics*” in contrast to Gibbs equilibrium thermodynamics or simply “*Hillert thermodynamics*” vs Gibbs thermodynamics. As mentioned in Section 2.1, one may thus define the *Hillert energy* by  $\Phi = G - \sum_{i=1}^c \mu_i N_i$  and re-write the combined law of thermodynamics as follows

$$d\Phi = -SdT + VdP - \sum_{i=1}^c N_i d\mu_i - Td_{ip}S \quad \text{Eq. 23}$$

Consequently, Eq. 20 and Eq. 23 may be termed as Hillert nonequilibrium thermodynamics in contrast to Gibbs equilibrium thermodynamics represented by Eq. 1 and Eq. 3.

For systems with multiple internal processes, the entropy production can be written as<sup>22,49</sup>

$$d_{ip}S = \frac{1}{T} \sum_{j=1}^m D_j d\xi_j \quad \text{Eq. 24}$$

where  $D_j$  and  $\xi_j$  are a pair of internal conjugate variables for the  $j^{\text{th}}$  internal process. However, Hillert<sup>22</sup> followed Onsager theorem by taking into account the possibility that those internal processes may interact with each other though he explicitly stated that “this is usually called ***phenomenological equation*** because it is not based on any physical model”. As to be discussed in Section 5, the internal variables of  $D_j$  and  $\xi_j$  represent *independent* internal processes and are

in analogy to the external variables of  $Y^a$  and  $X^a$  in Eq. 3. Eq. 20 can thus be re-written as follows

$$dU = \sum_{a=1}^n Y^a dX^a - \sum_{j=1}^m D_j d\xi_j \quad \text{Eq. 25}$$

$$D_j d\xi_j \geq 0 \quad \text{Eq. 26}$$

It should be remembered that the entropy change,  $dS$  in the first summation in Eq. 25 now includes the second summation in Eq. 25. Furthermore,  $d\xi_j$  may include more than one  $dX^a$  such as chemical reactions that Hillert discussed<sup>22</sup> where  $d\xi_j$  represents the amount of the products formed, and  $D_j$  is the weighted chemical potentials of products minus those of reactants so that the combined internal process is an independent one.

It is noted that Eq. 26 indicates that each internal process must result in positive entropy production<sup>49</sup>, while Hillert<sup>22</sup> stated that “the second law is derived only for the whole system”, which is less restrictive. This difference is due to whether the internal processes are independent of each other or not. In Eq. 25, each pair of  $Y^a$  and  $X^a$  is independent of each other, so is each pair of  $D_j$  and  $\xi_j$ . If not, they should be combined and be represented by one new pair of  $D'_j$  and  $\xi'_j$ , just like the chemical reactions discussed by Hillert<sup>22</sup>, resulting in  $D'_j d\xi'_j \geq 0$ . In analogy to Eq. 18, the entropy production of each independent internal process can be divided into four actions: (1) heat generation ( $d_{ip}Q$ ), (2) consumption of some components as reactants ( $dN_{r,j}$ ), (3) production of some components as products ( $dN_{p,k}$ ), and (4) reorganization of its configurations ( $d_{ip}S^{config}$ ), as follows<sup>32,36</sup>,

$$d_{ip}S = \frac{d_{ip}Q}{T} - \sum_j S_j dN_{r,j} + \sum_k S_k dN_{p,k} + d_{ip}S^{config} = \frac{D}{T} d\xi \quad Eq. 27$$

where  $S_j$  and  $S_k$  are the partial entropies of reactant  $j$  and product  $k$  of the internal process.

The last part of Eq. 27 is based on the *linear proportionality* approximation with  $D$  and  $d\xi$  being the driving force and progress of the internal process. This is crucial in developing the flux equations from Hillert nonequilibrium thermodynamics, i.e., Eq. 20 or Eq. 25. In reality, internal processes do not obey linear proportionality for longer time, and one can always select a small enough  $d\xi$  so the higher-order terms are negligible and then perform integrations along the pathways to obtain overall entropy production. On the other hand, to study the stability of an internal process or a system such as the limit of instability and critical points, one must include higher order terms beyond linear proportionality as discussed in detail by Hillert<sup>22</sup>. From Eq. 20 or Eq. 25, one can see that the internal energy is a function of all  $X^a$  and internal variables of  $\xi$ , i.e.,  $U(X^a, \xi)$ , so are all the potentials as the derivatives of  $U(X^a, \xi)$  with respect to its natural variables. This relationship enables the development of the theory of cross phenomena in Section 5.

### 3.2 Onsager theorem

Experimental observations show that the transport of one molar quantity can be driven by the gradients of both its conjugate potentials and non-conjugate potentials. Based on the thermoelectric phenomena where the electric current can be driven by both electric field and temperature gradient and vice versa and the *conjecture* by Thomson in 1854 that the cross

coefficients are equal, Onsager<sup>24</sup> proposed the phenomenological relations that any flux is proportional to all independent driving forces in the system as follows

$$J_{\xi_j}^{Onsager} = - \sum_k L_{\xi_j \xi_k} \nabla D_k \quad \text{Eq. 28}$$

where  $L_{\xi_j \xi_k}$  is the kinetic coefficient for the flux of molar quantity  $\xi_j$  due to  $\nabla D_k = D_k/\Delta z$  with the summation going over gradients of all potentials, where  $\Delta z$  is the distance of the unit transport process. Eq. 28 implies that all driving forces contribute to the flux of  $\xi_j$ , in an *apparent* accordance with experimental observations and gives the rate of entropy production,  $d_{ip}S$ , as follows

$$\frac{T}{V} d_{ip}S = -J_{\xi_j}^{Onsager} \nabla D_j = \nabla D_j \sum_k L_{\xi_j \xi_k} \nabla D_k \quad \text{Eq. 29}$$

From “the assumption of microscopic reversibility”<sup>24</sup>, Onsager articulated that the phenomenological coefficient matrix in Eq. 28 is symmetric, i.e.,

$$L_{\xi_j \xi_k} = L_{\xi_k \xi_j} \quad \text{Eq. 30}$$

It is important to note that the principle of microscopic reversibility implies that “the fluctuations in a system which has been left isolated for a length of time that is normally sufficient to secure thermodynamic equilibrium”<sup>24</sup>, which as pointed out by Onsager at the same time that “the reversible fundamental laws of dynamics are not compatible with absolutely irreversible processes”<sup>24</sup>.

It is thus evident that the Onsager theorem discussed above is not on a strong foundation and has been strongly criticized by Truesdell and co-workers<sup>62,63</sup>, while Hillert<sup>22</sup> emphasized its

*phenomenological* nature, and Balluffi et al.<sup>23</sup> mentioned that it is not as fundamental as the 1<sup>st</sup> and 2<sup>nd</sup> laws of thermodynamics which was also stated by Onsager himself<sup>24</sup> as quoted in the introduction of the present paper . The present author started to look into this during his sabbatical leave when worked on thermodiffusion with Murch and his team<sup>42–46</sup>, i.e., atomic diffusion driven by temperature gradient. Through molecular dynamics (MD) simulations, one can evaluate the Onsager phenomenological coefficients as time integrals of correlation functions involving the microscopic fluxes of atoms and heat using the Green–Kubo formulae<sup>42–46</sup>. This results in two coefficients for one component in a binary system as evidenced by Eq. 28. On the other hand, it is well-known that there is only one diffusivity for each diffusion component, namely its tracer diffusivity or atomic mobility in the lattice-fixed frame of reference<sup>64</sup>. This was puzzling to the author how these two could be reconciled. After seven years of investigations, the author developed the theory of cross phenomena by examining the inconsistencies in the Onsager theorem and deriving the flux equations from Hillert nonequilibrium thermodynamics as shown by Eq. 25, which is presented in Section 5.

### 3.3 Prigogine entropy balance

There are many efforts in further evaluating entropy production beyond Eq. 29 as shown by de Groot and Mazur<sup>65</sup>, Kondepudi and Prigogine<sup>66</sup>, and in most irreversible thermodynamics textbooks. Unfortunately, all of them started with the Gibbs equilibrium thermodynamics, i.e., Eq. 1 or Eq. 3, without realizing  $d_{ip}S = 0$ , by re-written it as follows

$$dS = \frac{1}{T} dU - \frac{1}{T} dW - \sum_{i=1}^c \frac{\mu_i}{T} dN_i \quad \text{Eq. 31}$$

For example, Kondepudi and Prigogine<sup>66</sup> considered a system without work, and Eq. 31 becomes

$$dS = \frac{1}{T}dU - \sum_{i=1}^c \frac{\mu_i}{T}dN_i = d_e S \quad \text{Eq. 32}$$

where the last portion was added in the present work with  $d_e S$  being the equilibrium entropy change or entropy current between the system and its surroundings <sup>66</sup>. Its time-dependent form can be written as

$$\frac{dS}{dt} = \dot{S} = \frac{1}{T}\dot{U} - \sum_{i=1}^c \frac{\mu_i}{T}\dot{N}_i = {}_e\dot{S} \quad \text{Eq. 33}$$

As discussed in detail in a recent publication by the present author <sup>33</sup>, Kondepudi and Prigogine <sup>66</sup> obtained the following through re-using the 1<sup>st</sup> law of thermodynamics

$$\dot{S} = {}_e\dot{S} = {}_e\dot{S} + {}_{ip}\dot{S} \quad \text{Eq. 34}$$

where  ${}_{ip}\dot{S}$  is the entropy production rate due to irreversible internal processes, written as  $\sigma$  by Kondepudi and Prigogine <sup>66</sup>. This is evidently incorrect because one cannot start with the equation applicable to equilibrium systems without internal processes and end up with an equation for nonequilibrium systems with internal processes because Eq. 34 implies that  ${}_{ip}\dot{S} = 0$ , which is defined in Gibbs equilibrium thermodynamics, i.e., Eq. 1, Eq. 3, Eq. 31, or Eq. 32. The problem is due to the circular use of the 1<sup>st</sup> law of thermodynamics as discussed by the present author <sup>33</sup>.

It is important to realize that the 1<sup>st</sup> law of thermodynamics does not concern the internal processes, but only the exchange between the system and its surroundings as shown by first part of Eq. 1. The insertion of entropy change into the 1<sup>st</sup> law of thermodynamics is based on Eq. 18 which shows that  $d_{ip}S$  is part of  $dS$  and thus must be subtracted in Eq. 20. While Eq. 3, Eq. 31, or Eq. 32 are valid only with  $d_{ip}S = 0$ , thus no internal processes in the system for entropy

production. In the extended irreversible thermodynamics<sup>67,68</sup> that includes fluxes as basic independent variables, Eq. 20 can be re-arranged as follows

$$\dot{S} = \frac{1}{T}\dot{U} - \frac{1}{T}\dot{W} - \sum_{i=1}^c \frac{\mu_i}{T}\dot{N}_i + {}_{ip}\dot{S} = {}_e\dot{S} + {}_{ip}\dot{S} \quad \text{Eq. 35}$$

with  ${}_{ip}\dot{S}$  related to the divergency of fluxes<sup>67,68</sup>. It remains how to define the flux equations.

### 3.4 Agren atomic mobility

In 1980s, the author learned from Agren<sup>69</sup> that each diffusion component has one diffusion mobility in the lattice-fixed frame of reference ( $M_i$ ), which can be related to its tracer diffusivity ( $D_i^*$ ) or kinetic coefficient ( $L_i$ ) in the linear relationship between its flux and chemical potential gradient. When this chemical potential gradient is changed to the concentration gradients of all independent diffusion components, one obtains a vector of intrinsic diffusivity in the lattice-fixed frame of reference ( ${}^iD_{ik} = L_i \frac{\partial \mu_i}{\partial c_k}$ ) due to the dependence of the chemical potential on the compositions of all components ( $c_k$ ). When the lattice-fixed frame of reference is changed to the volume-fixed frame of reference while keeping the chemical potential gradient, one obtains a kinetic coefficient vector ( $L'_{ij}$ ) due to the dependence of volume on all components. When both changes are made, one obtains the chemical or interdiffusion diffusivity vector ( $D_{ik} = \sum_j L'_{ij} \frac{\partial \mu_j}{\partial c_k}$ ).

Andersson and Ågren<sup>64</sup> presented an elegant discussion among all the diffusion coefficients and their computational implementation. The relationships among these kinetic coefficients are shown in Figure 1. It is thus clear that both the intrinsic and chemical diffusivity coefficients are



related to the mobility and thermodynamic factors defined by the derivatives between chemical potentials and compositions ( $\frac{\partial \mu_j}{\partial c_k}$ ) and are not independent kinetic coefficients as shown by the Maxwell-Stefan diffusion equation<sup>70,71</sup> and discussed by the present author<sup>33</sup>.

*Figure 1: Relationships among tracer diffusivity, atomic mobility, kinetic L parameters, and intrinsic and chemical diffusivities<sup>32</sup>.*

A large number of atomic mobility databases have since been developed with Gibbs energy functions modeled by the CALPHAD method<sup>72,73</sup> and used to simulate diffusional processes in multicomponent alloys, including joining of dissimilar materials<sup>74-76</sup>. One interesting scenario is when one component diffuses much faster than other components and thus takes much short time to reach the chemical equilibrium than other slow diffusion components, such as carbon (C) vs silicon (Si) in steels. Since the chemical potential of C is significantly affected by Si, the concentration of C can become more inhomogeneous than before, i.e. so-called uphill diffusion where C migrates from low C concentration to high C concentration regions, postulated and observed by Darken<sup>77-79</sup>. The uphill diffusion in Fe-Si-C alloys with inhomogeneous Si concentrations are successfully simulated by means of the mobility database and Dictra software developed by Agren and his team<sup>72,80</sup> and discussed in detail by the present author<sup>33</sup>. It is important to point out that C always diffuses from high to low chemical potential regions as its chemical potential is affected by the Si concentration which takes much longer time to be homogenized.

Another commonly observed uphill diffusion is when the solution is unstable with respect to composition fluctuations, referred to as spinodal decomposition<sup>81–84</sup>. The limit of stability of a solution is located at  $\frac{\partial \mu_i}{\partial c_i} = 0$ , and inside a spinodal the solution is unstable with  $\frac{\partial \mu_i}{\partial c_i} < 0$ , resulting in negative chemical diffusivity. The instability-driven spinodal decompositions play a central role in the formation of patterns<sup>66,83</sup>.

One important phenomenon in diffusion is the Kirkendall effect<sup>85–87</sup> due to the difference in fluxes of substitutional elements which results in a net vacancy flow and the formation of voids, which has also been successfully simulated using the atomic mobility databases together with thermodynamic databases<sup>88,89</sup>. The flux of vacancy,  $J_{Va}$ , can be written as follows

$$J_{Va} = - \sum_{i \in S} J_i \quad \text{Eq. 36}$$

where  $i \in S$  denotes all substitutional diffusion components, and  $J_i$  the flux of component  $i$ . It shows that the unbalanced fluxes of substitutional components can result in a net vacancy flow.

The atomic mobility databases have been mostly evaluated from the experimentally measured chemical diffusivity in combination with CALPHAD thermodynamic databases. The author's group developed a fully DFT-based approach to predict the tracer diffusivity in pure elements and dilute solutions for fcc<sup>90–94</sup>, bcc<sup>95</sup>, and hcp<sup>95–98</sup> phases based on the classic transition state theory (TST)<sup>99,100</sup>, the nudged elastic band (NEB) method<sup>101</sup>, and the five frequency model<sup>102</sup>, showing remarkable agreement with available experimental data. A similar approach was developed for prediction of interstitial diffusion coefficients in the literature at the same time<sup>103</sup>.

Using the thermodynamic and mobility databases, Höglund and Ågren<sup>104</sup> simulated C diffusion in steel driven by a temperature gradient under the framework of Onsager theorem by treating the coefficient in front of the temperature gradient as a constant. As it will be shown in Section 5.4.2, it should be the product of atomic mobility and the derivative of chemical potential with respect to temperature, thus dependent on both temperature and composition<sup>33</sup>.

## 4 Zentropy theory

### 4.1 Multiscale entropy and its coarse-graining

Experimentally, entropy can be obtained by the integration of measured heat capacity over temperature ( $C_p/T$ ) from 0 K to finite temperature using the 3<sup>rd</sup> law of thermodynamics stipulating  $S = 0$  at  $T = 0$  K. While in statistical mechanics, Eq. 13 represents the entropy of the system only when the configurations are pure quantum configurations with their entropy being zero. It is self-evident that if the entropies of individual configurations are not zero, their contributions to the total entropy of the system must be considered. It is postulated that the total entropy of the system can be written as follows<sup>36</sup>

$$S = \sum_{k=1}^m p^k S^k - k_B \sum_{k=1}^m p^k \ln p^k = \int_0^T \frac{C_p}{T} dT \quad \text{Eq. 37}$$

where  $S^k$  is the entropy of configuration  $k$ .

In principle, one can continuously dive into finer scale configurations until the pure quantum configuration is reached, which is intractable in today's computing capability due to too many configurations. One option is to stop at the scale of the ground-state configuration of the system defined by the DFT-based quantum mechanics as discussed in Section 2.2 and explore all non-

ground-state symmetry-broken configurations in terms of the internal degrees of freedom of the ground-state configuration. The free energy and entropy of each configuration can then be predicted by Eq. 10 to Eq. 12.

The usefulness of Eq. 37 relies on following two premises:

- The supercell size in DFT-based calculations based on today's computing capability is large enough to capture the electron and phonon interactions in the system so that each configuration can be treated as independent.
- The configurations are ergodic so that there are no unrepresented configurations when the configurations are thermally fluctuated in the system under the given external constraints.

These two premises are interconnected as the larger the supercell size, the more the number of configurations. In principle, convergency tests are needed in terms of the predicted properties of the system. Alternatively, comparison with experimental observations, if available, can be used as a guidance in order to save computing expenses.

In condensed matter physics, many phenomena are due to short-range interactions and can be represented by the supercell size and the corresponding number of configurations within today's computing capability. An alternative approach is to develop machine learning (ML) models from fewer DFT-based calculations and use them to predict properties of large supercells and a large number of configurations<sup>105,106</sup>.

## **4.2 Statistical mechanics based on the zentropy theory**

Applying Eq. 37 to a system of canonical ensemble under constant NVT, Eq. 14 to Eq. 16 are revised as follows

$$F = \sum_{k=1}^m p^k E^k - TS = \sum_{k=1}^m p^k F^k + k_B T \sum_{k=1}^m p^k \ln p^k \quad \text{Eq. 38}$$

$$Z = e^{-\frac{F}{k_B T}} = \sum_{k=1}^m Z^k = \sum_{k=1}^m e^{-\frac{F^k}{k_B T}} \quad \text{Eq. 39}$$

$$p^k = \frac{Z^k}{Z} = e^{-\frac{F^k - F}{k_B T}} \quad \text{Eq. 40}$$

As it can be seen,  $E^k$  in Eq. 14 to Eq. 16 is replaced by  $F^k$  in Eq. 38 to Eq. 40, and they are identical when  $S^k = 0$ . Eq. 37 to Eq. 40 was recently suggested to be termed as zentropy theory<sup>37</sup>, and its significances are discussed below.

For condensed matter, Eq. 37 integrates three scientific domains, i.e., quantum mechanics, statistical mechanics, and thermodynamics in terms of first summation, second summation, and the integration. The quantum mechanics and statistical mechanics communities have been largely separated from each other with the former focusing on the ground-state configurations and the latter based on Gibbs formalism. Efforts have been made to bridge the gaps between them through bottom-up approaches by considering the thermal electronic and phonon distributions of the ground-state configurations or using effective Hamiltonian fitted to DFT-based calculations and/or experimental observations followed by MD or Monte Carlo (MC) simulations. There are also limited work on *ab initio* molecular dynamic (AIMD) and quantum Monte Carlo (QMC) simulations. However, quantitative agreement between predictions and experiments is lacking in the literature due to the intrinsic limitations of existing approaches as

discussed in our recent publication <sup>41</sup>, i.e., the simultaneous considerations of all internal degrees of freedom and the ergodicity of independent configurations as a function of external constraints.

In the materials science and engineering discipline, the system of interest is at the microstructure level, consisting of individual phases and their temporal and spatial evolutions. To start with, one can take each individual phase as a subsystem of investigation and define its configurations in terms of atomic, magnetic, electrical, and defect configurations and predict its properties by means of the zentropy theory. These properties can then be used in phase-field methods to simulate their temporal and spatial evolutions <sup>83</sup>. Another important property needed for phase-field simulations is the interfacial energy between phases including grain boundary energy, and its accurate prediction is still lacking with similar reason mentioned in the previous paragraph <sup>41</sup>. One potential solution is to fit the effective Hamiltonian to free energies of all configurations predicted by the zentropy theory followed by MD or MC simulations. While this can account properly the first summation in Eq. 37 for interfaces, and additional steps are needed in treating the second summation in Eq. 37 so the total entropy can be accurately predicted.

### **4.3 Prediction of emergent behaviors in magnetic materials by zentropy theory**

#### *4.3.1 General discussion of emergent behaviors*

In the present work, emergent behaviors refer to abnormal responses of the system to external stimuli such as temperature, pressure, stress, strain, and electric and magnetic fields that are typically related to 1<sup>st</sup>, 2<sup>nd</sup>, and 3<sup>rd</sup> derivatives of free energy of the system. With the free energy of condensed matter accurately predicted by the zentropy theory as a function of both external and internal degrees of freedom, it is anticipated that their emergent behaviors can be predicted

accordingly. It can be seen from Eq. 37 and Eq. 38 that the nonlinear or emergent behaviors primarily originate from the logarithmic term, i.e., the statistical competition among configurations with respect to external stimuli.

Gibbs thermodynamics, i.e., Eq. 3, shows that the 1<sup>st</sup> derivative of energy with respect to a molar quantity gives its conjugate potential with other molar quantities as natural variables kept constant, i.e.,

$$Y^a = \frac{\partial U}{\partial X^a} \quad \text{Eq. 41}$$

By defining a free energy, such as Helmholtz energy for theoretic investigation of condensed matter in the present work, the 1<sup>st</sup> derivative with respect to temperature gives the negative of its conjugate molar quantity, entropy, i.e.,

$$S = -\frac{\partial F}{\partial T} \quad \text{Eq. 42}$$

The deviation of entropy from that of the ground-state configuration in terms of QHA phonon calculations is considered to be anharmonic <sup>107</sup>.

The 2<sup>nd</sup> derivatives of energy are defined by the 1<sup>st</sup> derivatives between molar quantities and potentials and are listed in Table 1, and between molar quantities and between potentials in Table 2. Both tables are symmetric due to the Maxwell relations based on the 2<sup>nd</sup> derivatives of free energy. The diagonal quantities in Table 1 are between conjugate variables and are positive for a stable system as shown by Eq. 9, while the off-diagonal quantities are between non-conjugate variables and can be either positive or negative such as negative thermal expansion in INVAR alloys <sup>108–110</sup>. The derivative between conjugate molar quantity and potential diverges positively

at the limit of stability, such as  $\frac{\partial S}{\partial T} = +\infty$  as discussed in Section 2.1, resulting the maximum anharmonicity. While the derivatives between non-conjugate molar quantity and potential diverge either positively or negatively at the limit of stability, i.e.,

$$\frac{\partial X^a}{\partial Y^b} = \frac{\partial X^b}{\partial Y^a} = \pm\infty \quad \text{Eq. 43}$$

Most of the quantities in Table 1 are well known properties except those in the last row and last column, which are related to chemical reactions where the amount of a component changes with respect to potentials. The author assigned some names to the quantities in the last row, but the names for those in the last column remain to be assigned.

*Table 1: Physical quantities related to 1<sup>st</sup> directives between molar quantities (first column) and potentials (first row), slightly modified from Ref. <sup>33</sup>.*

*Table 2: Cross phenomenon coefficients represented by 1<sup>st</sup> derivatives between potentials, slightly modified from Ref. <sup>33</sup>.*

The derivatives between potentials in Table 2 are less discussed in the literature though Gibbs <sup>3,4</sup> presented a number of them in connection with equilibria involving solid and interfaces between phases such as  $\frac{\partial \mu_i}{\partial T}$ ,  $\frac{\partial \mu_i}{\partial P}$ , and  $\frac{\partial P}{\partial T}$ , which were commonly referred as cross phenomena in the literature where the Onsager theorem was based on <sup>24,25</sup>. As a matter of fact, all off-diagonal quantities in Table 1 and Table 2 represent cross phenomena between non-conjugate variables and will be further discussed in connection with the theory of cross phenomena in Section 5.



### 4.3.2 Emergent behaviors in magnetic materials

Magnetic materials have been used in developing the zentropy theory starting with anti-invar Ce<sup>34,35</sup> due to its importance in Mg alloys<sup>111,112</sup>, followed by INVAR Fe<sub>3</sub>Pt due to its negative thermal expansion<sup>39,61,113,114</sup>, with the configurations defined by various magnetic spin configurations. Over the years, the author's group used the zentropy theory to predict the magnetic transitions in bcc-Fe<sup>115</sup>, fcc-Ni<sup>116</sup>, orthorhombic BaFe<sub>2</sub>As<sub>2</sub><sup>117-119</sup>, and YNiO<sub>3</sub><sup>41</sup>. An attempt was made recently to apply the zentropy theory to the ferroelectric transition in PbTiO<sub>3</sub> with encouraging results<sup>120</sup>.

The ground-state configuration of Ce is nonmagnetic (NM), and its room temperature phase is ferromagnetic (FM). We started with these two configurations with a one-atom supercell<sup>34</sup>, but had to add a mean-field magnetic spin flipping term in free energy as commonly done in the literature<sup>121</sup> in order to obtain the critical point in its T-P phase diagram. Since the co-existence of the NM and FM configuration results in spin-flipping magnetic (SFM) configurations and magnetic spin domain walls, an antiferromagnetic (AFM) configuration was added with a two-atom supercell<sup>35</sup>. With the Helmholtz energies of these three configurations obtained from DFT-based calculations, the critical point and associated anomalies were accurately predicted without the mean-field term<sup>35,38,61</sup>.

It was observed that the probability of the ground-state configuration is about 0.5, i.e.,  $p^g = 0.5$ , at the critical point with  $T_{cp} = 546 K$  and  $P_{cp} = 2.05 GPa$  within the range of experimental observations. The predicted T-P and T-V phase diagrams show remarkable agreement with

experimental observations with only inputs from DFT-based calculations thus free of fitting parameters<sup>35,37,61</sup>. The positive divergency of thermal expansion was predicted at the critical point, attributing to the larger volumes of the AFM and FM configurations than that of the NM ground-state configuration. This can be seen from the following equations for volume and thermal expansion of a system in terms of the zentropy theory<sup>122</sup>

$$V = \frac{\partial G}{\partial P} = \sum_{k=1}^m p^k V^k = V^g + \sum_{k=1}^m p^k (V^k - V^g) \quad \text{Eq. 44}$$

$$\frac{\partial V}{\partial T} = \sum_{k=1}^m \left[ p^k \frac{\partial V^k}{\partial T} + \frac{\partial p^k}{\partial T} (V^k - V^g) \right] \quad \text{Eq. 45}$$

where  $V^g$  and  $V^k$  are the volumes of the ground-state configuration and the configuration  $k$ , respectively. From Eq. 44, it can be seen that if  $V^k > V^g$ , one must have  $V > V^g$  due to  $p^k \geq 0$ . With  $\frac{\partial p^g}{\partial T} < 0$  for the ground-state configuration and  $\frac{\partial p^k}{\partial T} > 0$  for non-ground-state configurations, one has  $\frac{\partial V}{\partial T} > 0$ , so the divergence is also positive, i.e.,  $\frac{\partial V}{\partial T} = +\infty$ , as observed in the T-V phase diagram of Ce<sup>37,61</sup>.

It is immediately evident that if  $V^k < V^g$ , it is possible that  $V < V^g$  and  $\frac{\partial V}{\partial T} < 0$  under certain T and P ranges. This is indeed the case for Fe<sub>3</sub>Pt with the volume of its FM ground-state configuration larger than those of all SFM configurations<sup>39</sup>. Using a 12-atom supercell with  $2^9 = 512$  collinear SFM configurations, of which 37 is unique due to symmetry, the zentropy theory was able to accurately predict the T-P and T-V phase diagrams showing the FM to paramagnetic (PM) transition and the negative thermal expansion in a range of T and P combinations, showing remarkable agreement with experimental observations without fitting parameters<sup>39,61,113,114</sup>.

As in the case of Ce,  $p^g = 0.5$  is also observed at the critical point in Fe<sub>3</sub>Pt with  $T_{cp} = 141$  K and  $P_{cp} = 5.81$  GPa within the range of experimental observations<sup>39</sup>. Since a critical point is where the 1<sup>st</sup>- and 2<sup>nd</sup>-order transitions meet, it is convenient to define a 2<sup>nd</sup>-order transition by  $p^g = 0.5$ . On the other hand, the definition of a 2<sup>nd</sup>-order transition is by the discontinuity of the 2<sup>nd</sup>-order derivative of Helmholtz energy to T, i.e., heat capacity. In Ce, it was found that the maximum of the sum of the magnetic plus electronic heat capacities is at 500 K under 2.05 GPa, lower than 546 K with  $p^g = 0.5$  at the same pressure<sup>35</sup>. For bcc-Fe, the 2<sup>nd</sup>-order transition temperature is in the descending order of  $p^g = 0.5$ , the maximum of the total  $C_p$ , and the maximum of the magnetic heat capacity with the middle one in accordance with the agreed value in the literature from experimental measurements<sup>39</sup>. It is noted that the predicted heat capacity shows a maximum, but not a discontinuous jump with respect to temperature as shown by experimental observations, probably due to the small supercell size used in the DFT-based calculations.

In BaFe<sub>2</sub>As<sub>2</sub><sup>117-119</sup>, the ground-state configuration is a spin density wave (SDW) AFM configuration with a stripe like Fe spin ordering pattern within the *ab* plane and antiparallel nearest-neighbor Fe spins along the *c* axis of an orthorhombic structure. The predicted SDW ordering temperature with  $p^g = 0.5$  as a function of pressure, showing remarkable agreement with experimental measurements<sup>119</sup>. Furthermore, it was found that the temperature with  $p^g = 0.9999$  as a function of pressure is in accordance with a characteristic superconducting-like

temperature, which is in alignment with our postulations of superconductivity<sup>32</sup> though the superconducting configuration remains to be defined as part of our on-going investigations<sup>123</sup>.

#### 4.3.3 *On YNiO<sub>3</sub> with strongly correlated physics*

The phase transitions in the RNiO<sub>3</sub> family were investigated in the literature by using a combination of DFT and dynamical mean-field theory calculations<sup>124,125</sup>, where the critical role of strong correlation was emphasized. The zentropy theory was recently applied to predict the AFM-to-PM transition in YNiO<sub>3</sub><sup>41</sup>. The ground-state configuration of YNiO<sub>3</sub> is rather complex with half of the Ni atoms having a negligible magnetic moment and the other half arranged in an AFM configuration<sup>40</sup>. Had the YNiO<sub>3</sub> phase been considered nonmagnetic, its minimum cell would contain four ABO<sub>3</sub> formula units with 20 atoms. For magnetic spin configurations, a minimum cell of 16 formula units with 80 atoms is needed for its monoclinic P2<sub>1</sub>/n structure. There are 35 possible supercells in terms of the spatial arrangements of four 20-atom base cells. Restricting the initial spin configuration to be 8 Ni atoms with zero magnetic moments and 8 Ni atoms with nonzero magnetic moments creates 256 spin configurations for each supercell, of which 37 are symmetry-independent for the 80-atom 1×2×2 supercell.

With the Helmholtz energies of the 37 configurations predicted by DFT-based calculations, their probabilities are obtained using the zentropy theory as shown in Figure 2 (i) using  $F^k$  and (ii) using  $E^k$  for the partition function of each configuration, respectively, respectively. The predicted AFM-PM transition temperature of 144 K with  $p^g = 0.5$  using  $F^k$  agrees with the experimental value of 145 K, while the one using  $E^k$  results in a temperature of 81 K with  $p^g = 0.5$ . This difference is further shown in the  $T - P$  phase diagram in Figure 2 (iii). This

demonstrates the critical importance to include the phonon contributions to each configuration and revise the statistical mechanics using Helmholtz energy of each configuration in its partition function rather than the total energy. Figure 2 (iv) plots the magnetic spin short-range ordering (SRO) as a function of temperature under ambient pressure, showing that the AFM-to-PM transition is near the temperature where SRO is below 0.5. Here SRO is defined as the ratio between the standard deviations of the distribution of total magnetic moments around Ni atom within its 1<sup>st</sup> coordination sphere as computed by the zentropy theory and by the spin-special quasirandom model (i.e., the high-temperature limit of paramagnetic state) <sup>126,127</sup>.

It is thus demonstrated that the zentropy theory is capable of predicting the strongly correlated physics in YNiO<sub>3</sub> through the consideration of statistical mixture of the ground-state and non-ground-state configurations with their Helmholtz energies predicted by DFT-based calculations. It reveals the important role of spatial fluctuations, derived from the competition among spin ground-state and nonground-state configurations, in the AFM-to-PM phase transition.

Therefore, the strong correlations in YNiO<sub>3</sub> reside in each configuration and are exemplified by the spin and phonon interactions, while all configurations are coupled through statistical mechanics. It is thus critical to include the spin and phonon contributions in each configuration in statistical mechanics as in the zentropy theory to fully capture those strong correlated physics.

*Figure 2: YNiO<sub>3</sub> (i) predicted probabilities of the ground-state (red symbols) and non-ground-state (their sum in open symbols) configurations as a function of temperature under ambient pressure; (ii) same as (i) but with  $E^k$  instead of  $F^k$  for the partition function of configuration  $k$ ; (iii) predicted T-P phase diagram*

*superimposed with the AFM-to-PM transition temperature measured by experiments (red dot) and predicted using  $E^k$  (blue dot); (iv) predicted SRO as a function of temperature under ambient pressure* <sup>41</sup>.

#### 4.3.4 Miscalculation of entropy on “microscopic violation of second law of thermodynamics”

The violation of 2<sup>nd</sup> law of thermodynamics has been discussed in the literature since the 2<sup>nd</sup> law of thermodynamics was formulated. The latest argument was on the violation in the microscopic scale in the framework of fluctuation theorem <sup>128,129</sup>. Many theoretical, computational, and experimental investigations were performed aiming to demonstrate the existence of trajectories, with statistically significant probability, between two states of a system with the work done ( $\Delta W$ ) smaller than the equilibrium Helmholtz energy difference between the two states ( $\Delta F$ ) <sup>130–134</sup>.

Since the equilibrium Helmholtz energy difference between the two states represents the minimum amount of heat or work to move between these two states through reversible processes, the less amount of work observed indicates the violation of the 2<sup>nd</sup> law of thermodynamics. This means that a closed circle from one state to another state in a system by doing work  $\Delta W$  and then back to the original state by releasing the energy  $\Delta F$  would result in a net energy contribution, i.e.,  $(|\Delta F| - |\Delta W|) > 0$ , which could be extracted from the system. This was demonstrated by Maillet et al. <sup>133</sup> who extracted the amount of work up to large fractions of  $k_B T$  for a single-electron transistor two-level system with  $\Delta F = 0$  and a single thermodynamic trajectory level coupled to a single heat bath. However, Maillet et al. <sup>133</sup> pointed out that the requirement of an external intervention makes the 2<sup>nd</sup> law of thermodynamics remain valid.

More generally, the central question is how to fully count the entropy change for internal processes. By considering an internal process as a system, its entropy change between two moments and the total entropy at any moment are represented by Eq. 27 and Eq. 37, respectively. Using the reversible Brownian motion as an example, the author<sup>32</sup> pointed out that as soon as the probability for an atom to jump over to the next vacant site becomes statistically significant, additional entropy is introduced due to the 2<sup>nd</sup> summation in Eq. 37. The driving force for this internal reversible process is the thermal energy taken from its surroundings so Eq. 27 becomes

$$d_{ip}S = \frac{d_{ip}Q}{T} + d_{ip}S^{config} = 0 \quad Eq. 46$$

with  $d_{ip}Q < 0$  and  $Td_{ip}S^{config} = -d_{ip}Q$ . When the atom is at the next vacant site, the thermal energy is reversibly given back to its surroundings, leaving the entropies of both the internal process as a system and its surroundings unchanged.

It seems that in most discussions related to the “violation of second law of thermodynamics”, the 2<sup>nd</sup> summation in Eq. 37 is not included, resulting in incomplete accounting of entropy production represented by  $d_{ip}S^{config}$  so Eq. 46 becomes negative, thus a false conclusion on the violation of the 2<sup>nd</sup> law of thermodynamics.

## 5 Theory of cross phenomena

### 5.1 Issues on Onsager theorem and Prigogine entropy balance

Today’s irreversible thermodynamics are largely based on the Onsager theorem and Prigogine entropy balance. As discussed in Section 3.3, Prigogine entropy balance is based on Gibbs

equilibrium thermodynamics and can thus not be used to describe irreversible processes.

Furthermore, the irreversible thermodynamics established by Prigogine and co-workers<sup>66</sup> are based on Onsager theorem, which has several internal inconsistencies as discussed by the present author<sup>32,33</sup> and shown below in the present paper.

Through over seven years of study, the present author formulated four fundamental questions concerning the Onsager theorem as follows<sup>32,33</sup>

1. As a symmetric matrix can be diagonalized to obtain its eigen values (kinetic coefficients) and the eigen vector (the set of independent driving forces), what is the eigen vector after the diagonalization of Onsager flux equations?
2. When  $D_j = 0$ ,  $d\xi_j$  may not be zero because the Onsager flux equation relates  $d\xi_j$  to all driving forces. Does this mean that the internal processes are not independent?
3. The entropy production for the internal process in question 2 is zero as shown by Eq. 29, implying that  $J_{\xi_j}^{Onsager}$  does not produce entropy. Is this in conflict with the 2<sup>nd</sup> law of thermodynamics?
4. If the microscopic reversibility and Gibbs thermodynamics hold locally, so does the Gibbs-Duhem equation as shown by Eq. 6, signifying that not all potentials or their gradients could be varied independently. Does this mean at least one of the driving forces in Onsager flux equation is a molar quantity? If so, which one?

Phenomenological oriented approaches aim to correlate experimental observations with possible causes through the top-down macroscopic view of the responses of a system to the observer's



actions. For a more complete understanding of the responses, one must examine both the temporal and spatial resolutions of the observations and consider the internal processes in the system and the interactions between the system and its surroundings by microscopically eliminating the degrees of freedom and appropriately averaging the whole responses. The limited spatial resolution is very much similar to the parable of the blind men and the elephant articulated by Perdew et al.<sup>19</sup> that each individual observes a different portion of a complex system and thus is incomplete by themselves alone. This holistic view enabled Perdew and his collaborators<sup>13-19</sup> to develop the SCAN meta-GGA with significantly improved ground-state energetics as briefly discussed in Section 2.2. The limited temporal resolution is excellently illustrated by the illusion of thaumatrope where when a disk with a picture on each side is spined fast enough, the two pictures merge into one such as bird in the cage<sup>135</sup>.

This illusion was demonstrated by the transition of  $\text{PbTiO}_3$  from the ferroelectric tetragonal structure at low temperature to the paraelectric cubic structure at high temperature observed by X-ray and neutron diffractions. However, the ferroelectric tetragonal structure persists locally at both low and high temperatures as observed through the XAFS (x-ray-absorption fine structure) analysis with the time and spatial resolutions being  $\sim 10^{-16}$  sec (0.1 fs) and 1<sup>st</sup> to 4<sup>th</sup> nearest neighbor shells<sup>136-138</sup> and AIMD simulations<sup>139</sup> with the overall lattice parameters from the x-ray diffractions<sup>140</sup>. The faster switching of the ferroelectric tetragonal structure among different orientations at high temperature results in the macroscopic cubic structure observed by the x-ray diffractions with lower temporal and spatial resolutions as shown in the video from the AIMD simulations<sup>120</sup>.

As discussed below, the phenomenological Onsager flux equations originate from the dependence of a potential not only on its own conjugate molar quantity, but also on all other natural variables as mentioned in Section 3.1. Consequently, when one natural variable, whether it is a molar quantity or potential, is changed, the potentials of all other molar quantities are affected, resulting in driving forces for all other molar quantities to transport from their high potential regions to their respective low potential regions. Phenomenological correlations between the fluxes of those molar quantities to the change of the initial natural variable are similar to the illusions mentioned above. This is in analogy to a Chinese idiom: Move one hair and move the whole body.

## **5.2 Formulation of internal processes and entropy production**

The compact form of Hillert nonequilibrium thermodynamics is presented by Eq. 25 with the first summation denoting the interactions between the system and its surroundings and the second summation representing the *independent* internal processes. It is important to emphasize again that the entropy change in the first summation includes the total entropy production of all internal processes inside the system depicted by the second summation. For dependent internal processes such as chemical reactions discussed by Hillert<sup>22</sup>, Kondepudi and Prigogine<sup>66</sup>, and in Section 3.1, they should be combined when using the combined law of thermodynamics.

Eq. 25 shows only terms of products between conjugate variables without any cross-terms between non-conjugate variables. It is known that the equilibrium of a system is reached when each potential has the same value everywhere in the system. If this is not the case, the difference

of the potential provides the driving force for its conjugate molar quantity to migrate from high potential regions to low potential regions, resulting in a flux of the molar quantity in the system. This flux results in the change of other potentials in the system and provides driving forces for their molar quantities to migrate. Therefore, to answer the first question to Onsager theorem presented in Section 5.1 above, the eigen vector of driving forces is the gradient of all independent potentials shown by Eq. 25.

From the above discussion, the rate of the entropy production per volume due to the  $j^{th}$  internal process in a sufficiently small region with a thickness of  $\Delta z$  and area of  $A$  can be written as

$$\frac{T d_{ip} \dot{S}_j}{V} = \frac{D_j d \dot{\xi}_j}{A \Delta z} = -\frac{d \dot{\xi}_j}{A} \frac{\Delta Y_{\xi_j}}{\Delta z} = -\frac{d \dot{\xi}_j}{A} \nabla Y_{\xi_j} \quad Eq. 47$$

with  $D_j = -\Delta Y_{\xi_j}$  and  $Y_{\xi_j}$  being the conjugate potential of the internal variable of  $\xi_j$ , and  $\nabla Y_{\xi_j}$  the gradient of  $Y_{\xi_j}$ . The flux of  $\xi_j$ ,  $J_{\xi_j}$ , can then be defined as follows with the driving force being the gradient of its conjugate potential

$$J_{\xi_j} = \frac{d \dot{\xi}_j}{A} = -L_{\xi_j} \nabla Y_{\xi_j} \quad Eq. 48$$

where  $L_{\xi_j}$  is the kinetic coefficient for the change of  $\xi_j$ . Eq. 47 can be re-written as

$$\frac{T d_{ip} \dot{S}_j}{V} = L_{\xi_j} \left( \nabla Y_{\xi_j} \right)^2 \quad Eq. 49$$

It can be seen that Eq. 48 addresses both first and second questions to Onsager theorem presented in Section 5.1 above, i.e., the eigen vector being the potential gradients and a zero flux

of a molar quantity with a zero gradient of its conjugate potential. Eq. 49 answers the third question, i.e., zero entropy production for an internal process with a zero gradient of its potential.

The answer to the fourth question is more complex. As discussed by Hillert<sup>22</sup>, there are two types of stable equilibria with zero entropy productions with Eq. 26 written as

$$D_j d\xi_j = 0 \quad \text{Eq. 50}$$

with either  $D_j = 0$  or  $d\xi_j = 0$ . Hillert<sup>22</sup> termed the latter as equilibrium under freezing-in conditions when the internal process could not take place due to its high kinetic barrier in comparison to the thermal energy, and it is commonly referred as metastable equilibrium as the system free energy could be further reduced through some internal processes, such as diamond vs graphite.

For a homogeneous metastable system, the internal variable  $\xi_j$  becomes an independent variable of the system, and all the properties of the system are thus dependent on  $\xi_j$  as discussed by Hillert<sup>22</sup> and mentioned in Section 3.1. The Gibbs-Duhem equation, Eq. 6 or more precisely Eq. 23 or Eq. 25 with  $Td_{ip}S = \sum_{j=1}^m D_j d\xi_j = 0$ , is thus applicable to such a homogeneous system, i.e., the potentials in the system are not independent to each other. However, when there are internal processes inside the system  $Td_{ip}S > 0$ , Eq. 23 applies, and the Gibbs-Duhem equation is no longer valid.

Nevertheless, the free energy at each moment in time and space in the system with well-defined internal variables can be evaluated and used to calculate the properties through its derivatives,

while the change of free energy also depends on the change of the internal variables which are affected by all internal processes as shown by Eq. 25, resulting the cross phenomena that Onsager theorem aims to represent and are discussed in the next section.

### 5.3 Formulation of theory of cross-phenomena

As discussed above, each potential is a function of its conjugate molar quantity and all other natural variables of the system. Consequently, the gradient of a potential can be written in terms of the gradients of its conjugate molar quantity and all other natural variables with some of them being molar quantities and some of them being potentials as follows

$$\nabla Y_{\xi_j} = \frac{\partial Y_{\xi_j}}{\partial \xi_j} \nabla \xi_j + \sum_{\xi_k \neq \xi_j} \frac{\partial Y_{\xi_j}}{\partial Y_{\xi_k}} \nabla Y_{\xi_k} + \sum_{\xi_l \neq \xi_j, \xi_k} \frac{\partial Y_{\xi_j}}{\partial \xi_l} \nabla \xi_l \quad \text{Eq. 51}$$

where the first and second summations represent potential and molar quantity natural variables, respectively. In different experimental settings, one or more natural variables are controlled, but the summations in Eq. 51 must include all natural variables because their values will be affected by the changes of other natural variables internally. Those natural variables can be either all molar quantities or all potentials excluding  $Y_{\xi_j}$  and  $\xi_j$ .

The flux equation, Eq. 48, can thus be further expanded as follows

$$J_{\xi_j} = -L_{\xi_j} \nabla Y_{\xi_j} = -L_{\xi_j} \left( \frac{\partial Y_{\xi_j}}{\partial \xi_j} \nabla \xi_j + \sum_{\xi_k \neq \xi_j} \frac{\partial Y_{\xi_j}}{\partial Y_{\xi_k}} \nabla Y_{\xi_k} + \sum_{\xi_l \neq \xi_j, \xi_k} \frac{\partial Y_{\xi_j}}{\partial \xi_l} \nabla \xi_l \right) \quad \text{Eq. 52}$$

It is noted that  $L_{\xi_j}$  would also depend on all independent variables in Eq. 52, i.e.  $\xi_j$ ,  $Y_{\xi_k}$ , and  $\xi_l$ .

The two summations in Eq. 52 represent the cross phenomena in the system.

Eq. 52 is termed as the theory of cross phenomena <sup>32</sup>, and its significances are as follows

1. The flow of a molar quantity is *solely* driven by the gradient of its conjugate potential with a characteristic kinetic coefficient under the linear proportionality approximation, derived from the Hillert nonequilibrium thermodynamics *without phenomenological* considerations.
2. Both the potential gradient and the characteristic kinetic coefficient are functions of all independent variables in an internal process, resulting in the cross-phenomena shown by Eq. 52.
3. The product of the flux of a molar quantity and its conjugate potential results in the entropy production rate due to the internal process that contributes to the energy change rate of the system as one term in Hillert nonequilibrium thermodynamics.

The detailed applications of cross phenomena were discussed by the present author in the literature <sup>32</sup>, including thermoelectricity, thermodiffusion, chemical interdiffusion, electromigration, electrocaloric effect, and electromechanical effect. They are briefly reviewed and updated in following sections.

#### **5.4 Applications of theory of cross phenomena**

There are four common types of transport phenomena in condensed matter physics: heat, electron, mass, and fluid, commonly represented by the Fourier's, Ohm's, Fick's, and Darcy's laws based on experimental observations, with  $\xi_j = S, c_e, c_i$  and  $V$ , and  $\nabla Y_{\xi_j} = T, E, \mu_i$ , and  $-P$ , respectively. In the Fourier's, Ohm's, and Darcy's laws, Eq. 48 is used with the gradient of conjugate potentials as the driving force, so their linear proportionality coefficients represent the

kinetic coefficients, i.e.,  $L_{\xi_j}$  in Eq. 48. On the other hand, the concentration gradients, i.e.  $\nabla c_i$ , are used in Fick's law in terms of Eq. 52, which are not the true driving forces for diffusion.

Therefore, the kinetic coefficients  $L_{\xi_j}$ 's represent the direct relation between conjugate variables and discussed in detail by the present author<sup>32</sup>. The coefficients for cross-phenomena are the products of the kinetic coefficients and the thermodynamic properties represented by derivatives in Eq. 52. The derivatives between two potentials are relatively easy to measure as temperature, pressure, and electrical field are typically controlled experimentally, while the derivative between molar quantities can be predicted computationally<sup>22,38,49</sup>. This represents an integration of complimentary experimental and computational strengths connected by the Maxwell relation as follows

$$\frac{\partial Y^a}{\partial X^b} = \frac{\partial^2 \Phi}{\partial X^b \partial X^a} = \frac{\partial Y^b}{\partial X^a} \quad \text{Eq. 53}$$

$$\frac{\partial Y^a}{\partial Y^b} = \frac{\partial^2 \Phi}{\partial Y^b \partial X^a} = -\frac{\partial X^b}{\partial X^a} \quad \text{Eq. 54}$$

#### 5.4.1 Thermoelectricity

Thermoelectricity concerns the conduction of electrons or holes due to an externally applied temperature gradient. For electron and entropy conductions, the flux equations are written as follows

$$J_e = -L_e \nabla \mu_e \quad \text{Eq. 55}$$

$$J_S = -L_S \nabla T \quad \text{Eq. 56}$$

where  $L_e$  and  $L_S$  are the electrical and thermal conductivity, and  $\nabla\mu_e$  and  $\nabla T$  the gradients of chemical potential of electrons and temperature. Based on Hillert thermodynamics, the conjugate molar quantity of temperature is entropy rather than commonly used heat, and their relation is denoted by Eq. 18.

Let us conduct a virtual experiment to investigate the performance of a thermoelectric material as follows

- Initial condition at  $t = 0$  is with  $\nabla T = 0$ ,  $\nabla c_e = 0$ ,  $\nabla\mu_e = 0$ .
- At a very short time with  $t = \varepsilon$ , a temperature gradient is applied, resulting in  $\nabla T > 0$ . Assuming no electron migration yet, one has  $\nabla c_e = 0$ . However,  $\nabla\mu_e \neq 0$  due to the dependence of  $\mu_e$  on both electron concentration and temperature,  $\mu_e(c_e, T)$ .
- At  $t > \varepsilon$ : nonuniform  $\mu_e$  induces electron migration and results in a concentration gradient of electron in the thermoelectric material:  $\nabla c_e \neq 0$ .
- For open-circuit experimental setting, electrons remain in the system. For time long enough, the system reaches a steady state with  $J_e = 0$  and  $\nabla\mu_e = 0$ , balanced by  $\nabla c_e$  and  $\nabla T$ .
- The electron concentration profile in the system induces an internal electric field, and its voltage,  $\nabla V_e$ , can be measured.
- The ratio of voltage to  $\nabla T$  is determined and termed as Seebeck coefficient

$$S_{T,e} = \frac{\nabla V_e}{\nabla T} \quad \text{Eq. 57}$$

Re-writing Eq. 55 in terms of Eq. 52, one obtains



$$J_e = -L_e \nabla \mu_e = -L_e \left( \frac{\partial \mu_e}{\partial c_e} \nabla c_e + \frac{\partial \mu_e}{\partial T} \nabla T \right) = -L_e (\Phi_{ee} \nabla c_e - S_e \nabla T) \quad \text{Eq. 58}$$

where  $\Phi_{ee}$  and  $S_e$  are the thermodynamic factor and partial entropy of electrons. Under the steady state condition with  $J_e = 0$ , Eq. 58 gives

$$S_e = -\frac{\nabla V_e}{\nabla T} \quad \text{Eq. 59}$$

The combination of Eq. 57 and Eq. 59 results in the Seebeck coefficient

$$S_{T,e} = \frac{\nabla V_e}{\nabla T} = -S_e \quad \text{Eq. 60}$$

It is thus shown that the Seebeck coefficient for electron conduction, i.e., n-type of thermoelectric materials with electrons added to the conduction band, is negative of partial entropy of electrons. For p-type thermoelectric materials with positively charged holes added to the valence band, one has

$$J_h = -L_h (\nabla V_h - S_h \nabla T) = 0 \quad \text{Eq. 61}$$

$$S_{T,h} = \frac{\nabla V_h}{\nabla T} = S_h \quad \text{Eq. 62}$$

where  $L_h$ ,  $\nabla V_h$ ,  $S_h$ , and  $S_{T,h}$  are the kinetic coefficient, voltage, partial entropy, and Seebeck coefficient of holes in p-type thermoelectric materials, respectively. One thus has positive Seebeck coefficients for p-type thermoelectric materials. With the Helmholtz energy of electrons predicted by the DFT-based calculations (see Eq. 10 and Eq. 12), the author's group used the approach to accurately predict the Seebeck coefficients for several n- and p-type thermoelectric materials<sup>141,142</sup>.

Furthermore, the migrating electrons carry entropy with them, inducing an entropy current as follows

$$J_S = TS_e J_e = -TS_e L_e \nabla \mu_e \quad \text{Eq. 63}$$

This entropy current induced by the electrons in the charge current results in the Peltier effect with the Peltier coefficient defined by the division of entropy current to the electrical current as follows, noting that the electrical current is in the opposite direction of the electron flux

$$\Pi = \frac{J_S}{-J_e} = -TS_e = TS_{T,e} \quad \text{Eq. 64}$$

The Thomson relation between the Peltier and Seebeck coefficients comes out automatically

$$\Pi = TS_{T,e} \quad \text{Eq. 65}$$

The above discussion demonstrates that both Peltier and Seebeck coefficients are thermodynamic quantities related to the derivative of chemical potential of electron to temperature and equal to the partial entropy of electrons through the Maxwell relation as shown in Table 2 and as follows

$$S_{T,e} = \frac{\partial \mu_e}{\partial T} = \frac{\partial^2 G}{\partial T \partial c_e} = -\frac{\partial S}{\partial c_e} = -S_e \quad \text{Eq. 66}$$

#### 5.4.2 Thermodiffusion

Thermodiffusion is similar to thermoelectricity by changing the electrons to atoms and can be studied using the same virtual experiment presented in Section 5.4.1 above. The additional complexity is the dependence of the chemical potential on the concentrations of all components and the change of volume with respect to temperature, both affect atomic migration significantly. due to the second summation in Eq. 52. Consequently, the flux equation of thermodiffusion is written as

$$J_i = -L_i \nabla \mu_i = -L_i \left( \sum_j \Phi_{ij} \nabla c_j - P_i \nabla V - S_i \nabla T \right) \quad \text{Eq. 67}$$

For non-ideal solutions,  $L_i$ ,  $\Phi_{ij}$ ,  $P_i$ , and  $S_i$  can strongly depend on temperature and compositions of the solutions, resulting in a diffusion component switching their segregation regions as a function of composition and temperature<sup>143–150</sup> and also the Kirkendall effect as shown by Eq. 36 in Section 3.4.

For binary systems where most experiments are reported in the literature, Eq. 67 is written as follows

$$J_A = -L_A \nabla \mu_A = -L_A (\Phi_{AA} \nabla c_A + \Phi_{AB} \nabla c_B - P_A \nabla V - S_A \nabla T) \quad \text{Eq. 68}$$

$$J_B = -L_B \nabla \mu_B = -L_B (\Phi_{BA} \nabla c_A + \Phi_{BB} \nabla c_B - P_B \nabla V - S_B \nabla T) \quad \text{Eq. 69}$$

Under steady state conditions with  $J_A = J_B = 0$ , eliminating  $\nabla c_A$  from the equations results in

$$(\Phi_{BB} \Phi_{AA} - \Phi_{AB} \Phi_{BA}) \nabla c_B = (P_B \Phi_{AA} - P_A \Phi_{BA}) \nabla V + (S_B \Phi_{AA} - S_A \Phi_{BA}) \nabla T \quad \text{Eq. 70}$$

The Soret coefficient<sup>151</sup> is commonly defined by the negative ratio of the  $\nabla c_B$  with respect to  $\nabla T$  as follows

$$S_{T,B} = -\frac{\nabla c_B}{c_B \nabla T} = -\frac{1}{c_B} \frac{S_B \Phi_{AA} - S_A \Phi_{BA}}{\Phi_{BB} \Phi_{AA} - \Phi_{AB} \Phi_{BA}} \left( 1 + \frac{P_B \Phi_{AA} - P_A \Phi_{BA}}{S_B \Phi_{AA} - S_A \Phi_{BA}} \frac{\nabla V}{\nabla T} \right) \quad \text{Eq. 71}$$

Eq. 71 shows that  $S_{T,B} = 0$  when the one of the following conditions is met

$$S_B \Phi_{AA} - S_A \Phi_{BA} = 0 \quad \text{Eq. 72}$$

$$S_B \Phi_{AA} - S_A \Phi_{BA} + (P_B \Phi_{AA} - P_A \Phi_{BA}) \frac{\nabla V}{\nabla T} = 0 \quad \text{Eq. 73}$$

For systems with negative thermal expansion at certain composition and temperature ranges, it is possible that the Soret coefficient changes its sign with respect to composition and temperature as observed in the literature<sup>37,38,113</sup>.

The entropy flow due to atomic diffusions can be obtained by generalizing Eq. 63 as follows

$$J_S = T \sum_i S_i J_i \quad \text{Eq. 74}$$

This entropy flux contributes to the total entropy flux though very small due to the small flux in typical atomic diffusion.

While there are many discussions in the literature on Soret effects as reviewed by the present author<sup>32</sup>, the actual quantitative simulations of thermodiffusion is rare due to the lack of thermodynamic and kinetic databases. One very interesting work was reported by Höglund and Ågren<sup>104</sup> who simulated the thermodiffusion of carbon in an Fe-32%Ni-0.14%C (weight percent, wt%) alloy using available thermodynamic and mobility databases as discussed in Section 3.4. As discussed in detail by the present author<sup>32</sup>, it seems that their simulations can be further improved by connecting the commonly used heat of transport for component  $i$ ,  $Q_i^*$ , to its partial entropy as shown in Eq. 67, i.e.,

$$Q_i^* = T \frac{\partial \mu_i}{\partial T} = -TS_i \quad \text{Eq. 75}$$

### 5.4.3 Electromigration

Electromigration concerns the atomic diffusion driven by an external electrical field and is the most serious reliability issue in interconnect metallization and flip chip solder joints in electronic devices<sup>152–155</sup>. The initial internal process in electromigration is the electrical current, followed by entropy conduction, internal stress, and atomic diffusion. The flux for electromigration can be written as follows based on Eq. 52

$$J_i = -L_i \nabla \mu_i = -L_i \left( \sum_j \Phi_{ij} \nabla c_j - S_i \nabla T - \boldsymbol{\varepsilon}_i \nabla \boldsymbol{\sigma} - \boldsymbol{\theta}_i \nabla \mathbf{E} \right) \quad \text{Eq. 76}$$

where partial strain  $\boldsymbol{\varepsilon}_i$  and partial electrical displacement  $\boldsymbol{\theta}_i$  are listed in Table 2. The Kirkendall effect shown by Eq. 36 is more profound in electromigration as the electric field heavily affects migration directions of atoms with some models even including a source term for the nonequilibrium vacancy concentration<sup>156,157</sup>.

For electromigration of pure metals with approximations of  $\theta_i \approx 0$ ,  $\nabla c_j \approx 0$ ,  $\nabla T \approx 0$  and  $\nabla \boldsymbol{\sigma} \approx 0$ . With the internal electric field represented by the electron concentration as discussed in Section 5.4.1, Eq. 76 can be approximated as follows in analogy to Eq. 58

$$J_A = -L_A \nabla \mu_A = -L_A \frac{\partial \mu_A}{\partial c_e} \nabla c_e = -L_A \Phi_{Ae} \nabla c_e \quad \text{Eq. 77}$$

Therefore, pure metals diffuses in the same direction of the decrease of electron concentration, i.e. the direction of electron flow, from cathode to anode, and the vacancy diffuses in the opposite direction ( $J_{Va} = -J_A$ , see Eq. 36) resulting in the formation of voids on the cathode side<sup>152</sup>. The entropy flow can be calculated by Eq. 76 with the summation including both the element and electron.

#### 5.4.4 Electrocaloric effect

The electrocaloric effect (ECE) concerns the cross phenomenon between entropy conduction due to electron flow and an external electrical field for heating or cooling<sup>158–164</sup>. When an external electrical field is applied to the system, an electric current is generated due to the Ohm's law, and the electrons carry entropy with them, resulting in a conduction in terms of Eq. 63 due to the

electric current and Eq. 53 due to the temperature gradient. Considering only the flows of entropy and electrons, the entropy flux can be obtained from the general form of Eq. 52 as follows

$$J_S = -L_S \nabla T = -L_S \left( \frac{\partial T}{\partial S} \nabla S + \frac{\partial T}{\partial E} \nabla E \right) = -L_S \left( \frac{T}{C_p} \nabla S - \frac{1}{S_\theta} \nabla E \right) \quad \text{Eq. 78}$$

The derivatives in Eq. 78 are related to heat capacity and partial entropy with respect to electric displacement as depicted in Table 1 and Table 2, respectively.

Furthermore, the derivatives in Eq. 78 represent the direct and indirect methods used in the literature to characterize the ECE materials. In the direct method, the temperature increase under the *adiabatic condition* as a function of electric field is measured, i.e.  $(\Delta T / \Delta E)_{\Delta Q=0}$ . The adiabatic condition with  $\Delta Q = 0$  is identical to the isentropic condition with  $\Delta S = 0$  for a closed equilibrium system. The temperature change can be obtained through integration of the second derivative in Eq. 78 as follows

$$\Delta T_{direct} = \int_{E_1}^{E_2} \frac{\partial T}{\partial E} dE = - \int_{E_1}^{E_2} \frac{1}{S_\theta} dE \quad \text{Eq. 79}$$

In the indirect method, the heat production under the *isothermal condition* as a function of electrical field is measured, i.e.  $(\Delta Q / \Delta E)_T$  with  $\Delta Q$  treated to be the same as  $T \Delta S$ . The entropy change in the indirect method can be calculated through integration and is then used to calculate the anticipated temperature increase using the inverse of the first derivative in Eq. 78 or heat capacity of the materials as follows

$$\Delta S_{indirect} = \int_{E_1}^{E_2} \frac{\partial S}{\partial E} dE = \int_{T_1}^{T_1 + \Delta T_{indirect}} \frac{\partial S}{\partial T} dT = \int_{T_1}^{T_1 + \Delta T_{indirect}} \frac{C_P}{T} dT \quad Eq. 80$$

It is interesting to note that the results from both methods contribute to the entropy flow per Eq. 78. Therefore, maximizing both  $\Delta T_{direct}$  and  $\Delta S_{indirect}$  can improve the performance of ECE materials. Furthermore, while  $\Delta T_{direct}$  and  $\Delta T_{indirect}$  can both be used to characterize the performance of ECE materials, they are likely different from each other since both methods start from the same state, i.e.  $(T_1, S_1, E_1)$ , but end at different states, i.e.  $(T_1 + \Delta T_{direct}, E_2)_{S_1}$  vs  $(S_1 + \Delta S, E_2)_{T_1}$ . Therefore, it is in general that  $\Delta T_{indirect} \neq \Delta T_{direct}$ . Eq. 80 is often approximated in the literature by the following equation

$$T_1 \Delta S_{indirect} = C_P \Delta T_{indirect} \quad Eq. 81$$

This can introduce large errors due to the dramatic temperature dependence of  $C_P$  near morphotropic phase boundaries (MPBs) where ECE is mostly investigated.

#### 5.4.5 Electromechanical effect

The electromechanical effect concerns the interactions between electric field and elastic deformation usually under isothermal condition without atomic diffusion<sup>165–169</sup> with giant electromechanical effects observed near MPBs<sup>170–173</sup>. In piezoelectricity, electric charge is accumulated in response to externally applied stress, resulting in the electric current as follows

$$J_e = -L_e \nabla \mu_e = -L_e \left( \frac{\partial \mu_e}{\partial c_e} \nabla c_e + \frac{\partial \mu_e}{\partial \sigma} \nabla \sigma \right) = -L_e (\Phi_{ee} \nabla c_e - \varepsilon_e \nabla \sigma) \quad Eq. 82$$

where  $\varepsilon_e = \frac{\partial \varepsilon}{\partial c_e} = -\frac{\partial \mu_e}{\partial \sigma}$  is the partial strain with respect to electron concentration, included in

Table 2. Under the condition of zero electrical current, the voltage generated is as follows

$$\nabla V_e = \varepsilon_e \nabla \sigma \quad \text{Eq. 83}$$

In the converse piezoelectric effect, the elastic deformation is induced by an externally applied electric field. The mechanical equilibrium can be defined by vanishing stress gradient as follows

$$\nabla \sigma = \frac{\partial \sigma}{\partial \varepsilon} \nabla \varepsilon + \frac{\partial \sigma}{\partial c_e} \nabla c_e + \frac{\partial \sigma}{\partial E} \nabla E = 0 \quad \text{Eq. 84}$$

The zero electric current is written as follows

$$\nabla \mu_e = \frac{\partial \mu_e}{\partial c_e} \nabla c_e + \frac{\partial \mu_e}{\partial \varepsilon} \nabla \varepsilon + \frac{\partial \mu_e}{\partial E} \nabla E = 0 \quad \text{Eq. 85}$$

The partial derivatives in Eq. 84 and Eq. 85 are all included in Table 1 and Table 2. The giant electromechanical effects thus originate from the anomalies of these partial derivatives, which can be predicted by the zentropy theory if their configurations can be defined.

## 6 Summary and outlooks

In the present work, three distinct scientific domains developed in last 150 years are briefly reviewed, i.e., and equilibrium and nonequilibrium thermodynamics, statistical mechanics, and quantum mechanics. They have been largely separated from each other due to the different principles that each is based on and the different aspects of a complex system that each represents. Gibbs equilibrium thermodynamics inserts the entropy into the combined law of thermodynamics, and Hillert nonequilibrium thermodynamics adds the entropy production due to internal processes into the combined law of thermodynamics. Statistical mechanics depicts a top-down view of a system by considering configurations that the system is composed of and their statistical distributions in the system through partition functions of the system and individual configurations. Quantum mechanics in the framework of DFT focus on the electronic



structures, energetics, and phonon properties of the ground-state configuration of the system, aiming to predict the system behaviors from bottom-up.

The zentropy theory developed by the present author's group integrates DFT and statistical mechanics through following concepts and procedures

- Postulate that the configurations of a system are composed of the ground-state configuration from DFT and the non-ground-state configurations due to the internal degrees of freedom of the ground-state configuration, and the system at high temperature is a statistical mixture of all configurations.
- Examine all the configurations of the system in terms of multiplicity and stability and predict their Helmholtz energies as a function of external constraints through DFT-based calculations.
- Define the entropy of the system as the statistical entropy among all configurations plus the sum of the entropy of each configuration weighted by its statistical probability.
- Implement the revised statistical mechanics formalism by using the Helmholtz energy for the partition function of each configuration instead of commonly used total energy.
- Minimize the Helmholtz energy of the system with respect to internal degrees of freedom to obtain its equilibrium state with respect to external constraints.

It is demonstrated that the zentropy theory can accurately predict Helmholtz energy of several magnetic materials and all other properties derived from Helmholtz energy such as T-P and T-V phase diagrams with critical points, 1<sup>st</sup>- and 2<sup>nd</sup>-order magnetic transitions, anomaly in

thermodynamic properties, and positive and negative divergencies of thermal expansion, showing remarkable agreement with experimental observations.

Through analysis of Hillert nonequilibrium thermodynamics, it is concluded that the flux of a molar quantity is proportional *only* to the gradient of its conjugate potential rather than the gradients of all potentials in the phenomenological Onsager theorem. It is shown that the observed dependence of the flux on the gradients of other potentials is due to the dependences of the conjugate potential on the other potentials in the system. These dependences are represented by the derivatives between potentials. With the free energy of the system accurately predicted by the zentropy theory, those derivatives can be accurately predicted as demonstrated for Seebeck coefficients of several n- and p-type thermoelectric materials. It is shown that the closer a system to a critical point or phase boundary, the larger those derivatives, resulting in giant responses of a system to external stimuli.

There remain many challenging and complex problems to test the zentropy theory and the theory of cross phenomena in either smaller or larger systems. For smaller systems, one challenge is on superconductivity. Based on the success of the zentropy theory for magnetic materials, the present author presented several postulations on superconductivity with the focus on the search for the superconducting-state configuration as the ground-state configuration of a superconductor<sup>32</sup> with ongoing research activities<sup>123</sup>.

While for larger and more complex systems beyond the current DFT-based calculations, such as plants, organisms, forests, societies, planets, the solar system, black holes, galaxies, and

superclusters, there exist many intermediate levels of configurations between their ground-state configurations and observables. One potential approach is to take the inputs from both bottom-up quantum mechanics and top-down observations and cast them into the nested formula of the zentropy theory to develop practical solutions<sup>33,36</sup>.

Another potential direction is to improve the accuracy of MD simulations through the inclusion of configurational entropy among configurations in evaluating the total entropy of the system as briefly mentioned in Section 4.2 for interfacial energy. This is particularly interesting for predicting the properties of liquid or amorphous where the configurations are not well defined as in crystals. The present author and his collaborators are working on addressing this issue through prediction of melting using the zentropy theory, aiming to capture the total entropy and free energy of liquid more accurately.

## **7 Acknowledgements**

The author feels privileged to work with all his current and former students and numerous collaborators over the years at Penn State and around the world as reflected by the co-author names in the references cited in this paper. The present review article covers research outcomes supported by multiple funding agencies over multiple years as reflected in acknowledgements of the references cited. The most recent ones including the Endowed Dorothy Pate Enright Professorship at the Pennsylvania State University, U.S. Department of Energy (DOE) Grant No. DE-SC0023185, DE-AR0001435, DE-NE0008945, and DE-NE0009288, U.S. National Science Foundation (NSF) Grant No. NSF-2229690, NSF-2226976, and NSF-2050069, and Office of Naval Research (ONR) Grant No. N00014-21-1-2608 and N00014-23-2721.

## 8 References

1. Gibbs, J. W. *The collected works of J. Willard Gibbs: Vol. I Thermodynamics*. (Yale University Press, Vol. 1, 1948).
2. Gibbs, J. W. Graphical methods in the thermodynamics of fluids. *Trans. Connect. Acad. II April-May*, 309–342 (1873).
3. Gibbs, J. W. On the equilibrium of heterogeneous substances. *Trans. Connect. Acad. III May*, 108–248 (1876).
4. Gibbs, J. On the equilibrium of heterogeneous substances. *Trans. Connect. Acad. III July*, 343–524 (1878).
5. Gibbs, J. W. *The collected works of J. Willard Gibbs: Vol. II Statistical Mechanics*. (Yale University Press, Vol. II, 1948).
6. Schrödinger, E. An Undulatory Theory of the Mechanics of Atoms and Molecules. *Phys. Rev.* **28**, 1049–1070 (1926).
7. Landau, L. D. & Lifshitz, E. M. *Statistical Physics*. (Pergamon Press Ltd., 1970).
8. Hohenberg, P. & Kohn, W. Inhomogeneous electron gas. *Phys. Rev. B* **136**, B864–B871 (1964).
9. Kohn, W. & Sham, L. J. Self-Consistent Equations Including Exchange and Correlation Effects. *Phys. Rev.* **140**, A1133–A1138 (1965).
10. Langreth, D. C. & Perdew, J. P. Theory of nonuniform electronic systems. I. Analysis of the gradient approximation and a generalization that works. *Phys. Rev. B* **21**, 5469–5493 (1980).
11. Perdew, J. P., Chevary, J. A., Vosko, S. H., Jackson, K. A., Pederson, M. R., Singh, D. J. & Fiolhais, C. Atoms, molecules, solids, and surfaces: Applications of the generalized gradient approximation for exchange and correlation. *Phys. Rev. B* **46**, 6671–6687 (1992).
12. Perdew, J. P. & Wang, Y. Accurate and simple analytic representation of the electron-gas correlation energy. *Phys. Rev. B* **45**, 13244 (1992).
13. Sun, J., Ruzsinszky, A. & Perdew, J. Strongly Constrained and Appropriately Normed Semilocal Density Functional. *Phys. Rev. Lett.* **115**, 036402 (2015).
14. Furness, J. W., Kaplan, A. D., Ning, J., Perdew, J. P. & Sun, J. Accurate and Numerically Efficient r2SCAN Meta-Generalized Gradient Approximation. *J. Phys. Chem. Lett.* **11**, 8208–8215 (2020).
15. Grimme, S., Hansen, A., Ehlert, S. & Mewes, J. M. R2SCAN-3c: A ‘swiss army knife’ composite electronic-structure method. *J. Chem. Phys.* **154**, 64103 (2021).
16. Kothakonda, M., Kaplan, A. D., Isaacs, E. B., Bartel, C. J., Furness, J. W., Ning, J., Wolverton, C., Perdew, J. P. & Sun, J. Testing the r 2 SCAN Density Functional for the Thermodynamic Stability of Solids with and without a van der Waals Correction. *ACS Mater. Au* **3**, 102–111 (2023).
17. Perdew, J. P., Chowdhury, S. T. U. R., Shahi, C., Kaplan, A. D., Song, D. & Bylaska, E. J. Symmetry Breaking with the SCAN Density Functional Describes Strong Correlation in the Singlet Carbon Dimer. *J. Phys. Chem. A* **127**, 384–389 (2023).
18. Maniar, R., Withanage, K. P. K., Shahi, C., Kaplan, A. D., Perdew, J. P. & Pederson, M. R. Symmetry Breaking and Self-Interaction Correction in the Chromium Atom and Dimer. *J. Chem. Phys.* **submitted**, (2023).
19. Perdew, J. P., Ruzsinszky, A., Sun, J., Nepal, N. K. & Kaplan, A. D. Interpretations of

- ground-state symmetry breaking and strong correlation in wavefunction and density functional theories. *Proc. Natl. Acad. Sci. U. S. A.* **118**, e2017850118 (2021).
20. Mermin, N. D. Thermal Properties of the Inhomogeneous Electron Gas. *Phys. Rev.* **137**, A1441–A1443 (1965).
  21. Wang, Y., Liu, Z. K. & Chen, L.-Q. Thermodynamic properties of Al, Ni, NiAl, and Ni<sub>3</sub>Al from first-principles calculations. *Acta Mater.* **52**, 2665–2671 (2004).
  22. Hillert, M. *Phase Equilibria, Phase Diagrams and Phase Transformations*. (Cambridge University Press, 2007). doi:10.1017/CBO9780511812781
  23. Balluffi, R. W., Allen, S. M. & Carter, W. C. *Kinetics of Materials*. (John Wiley and Sons, 2005). doi:10.1002/0471749311
  24. Onsager, L. Reciprocal Relations in Irreversible Processes, I. *Phys. Rev.* **37**, 405–426 (1931).
  25. Onsager, L. Reciprocal relations in irreversible processes. II. *Phys. Rev.* **37**, 2265–2279 (1931).
  26. Prigogine, I., Outer, P. & Herbo, C. Affinity and Reaction Rate Close to Equilibrium. *J. Phys. Colloid Chem.* **52**, 321–331 (1948).
  27. Prigogine, I. The Equilibrium Hypothesis in Chemical Kinetics. *J. Phys. Chem.* **55**, 765–774 (1951).
  28. Prigogine, I. & Résibois, P. On the kinetics of the approach to equilibrium. *Physica* **27**, 629–646 (1961).
  29. Prigogine, I. & Nicolis, G. On Symmetry-Breaking Instabilities in Dissipative Systems. *J. Chem. Phys.* **46**, 3542–3550 (1967).
  30. Prigogine, I. Dissipative structures, dynamics and entropy. *Int. J. Quantum Chem.* **9-S9**, 443–456 (1975).
  31. Prigogine, I. Time, structure, and fluctuations. *Science* **201**, 777–785 (1978).
  32. Liu, Z. K. Theory of cross phenomena and their coefficients beyond Onsager theorem. *Mater. Res. Lett.* **10**, 393–439 (2022).
  33. Liu, Z. K. Thermodynamics and its prediction and CALPHAD modeling: Review, state of the art, and perspectives. *CALPHAD* **82**, 102580 (2023).
  34. Wang, Y., Hector, L. G., Zhang, H., Shang, S. L., Chen, L. Q. & Liu, Z. K. Thermodynamics of the Ce  $\gamma$ - $\alpha$  transition: Density-functional study. *Phys. Rev. B* **78**, 104113 (2008).
  35. Wang, Y., Hector Jr, L. G., Zhang, H., Shang, S. L., Chen, L. Q. & Liu, Z. K. A thermodynamic framework for a system with itinerant-electron magnetism. *J. Phys. Condens. Matter* **21**, 326003 (2009).
  36. Liu, Z. K., Li, B. & Lin, H. Multiscale Entropy and Its Implications to Critical Phenomena, Emergent Behaviors, and Information. *J. Phase Equilibria Diffus.* **40**, 508–521 (2019).
  37. Liu, Z. K., Wang, Y. & Shang, S.-L. Zentropy Theory for Positive and Negative Thermal Expansion. *J. Phase Equilibria Diffus.* **43**, 598–605 (2022).
  38. Liu, Z. K. Computational thermodynamics and its applications. *Acta Mater.* **200**, 745–792 (2020).
  39. Wang, Y., Shang, S. L., Zhang, H., Chen, L.-Q. & Liu, Z.-K. Thermodynamic fluctuations in magnetic states: Fe<sub>3</sub>Pt as a prototype. *Philos. Mag. Lett.* **90**, 851–859 (2010).
  40. Du, J., Shang, S.-L., Wang, Y., Zhang, A., Xiong, S., Liu, F. & Liu, Z.-K. Underpinned

- exploration for magnetic structure, lattice dynamics, electronic properties, and disproportionation of yttrium nickelate. *AIP Adv.* **11**, 015028 (2021).
41. Du, J., Malyi, O. I., Shang, S.-L., Wang, Y., Zhao, X.-G., Liu, F., Zunger, A. & Liu, Z.-K. Density functional thermodynamic description of spin, phonon and displacement degrees of freedom in antiferromagnetic-to-paramagnetic phase transition in YNiO<sub>3</sub>. *Mater. Today Phys.* **27**, 100805 (2022).
  42. Evteev, A. V., Levchenko, E. V., Belova, I. V., Kozubski, R., Liu, Z. K. & Murch, G. E. Thermotransport in binary system: case study on Ni 50 Al 50 melt. *Philos. Mag.* **94**, 3574–3602 (2014).
  43. Levchenko, E. V., Evteev, A. V., Ahmed, T., Kromik, A., Kozubski, R., Belova, I. V., Liu, Z.-K. & Murch, G. E. Influence of the interatomic potential on thermotransport in binary liquid alloys: case study on NiAl. *Philos. Mag.* **96**, (2016).
  44. Ahmed, T., Wang, W. Y., Kozubski, R., Liu, Z.-K., Belova, I. V. & Murch, G. E. Interdiffusion and thermotransport in Ni–Al liquid alloys. *Philos. Mag.* **98**, 2221–2246 (2018).
  45. Tang, J., Xue, X., Yi Wang, W., Lin, D., Ahmed, T., Wang, J., Tang, B., Shang, S., Belova, I. V., Song, H., Murch, G. E., Li, J. & Liu, Z. K. Activation volume dominated diffusivity of Ni<sub>50</sub>Al<sub>50</sub> melt under extreme conditions. *Comput. Mater. Sci.* **171**, 109263 (2020).
  46. Belova, I. V., Liu, Z.-K. & Murch, G. E. Exact phenomenological theory for thermotransport in a solid binary alloy. *Philos. Mag. Lett.* **101**, 123–131 (2021).
  47. Gibbs, J. W. Method of geometrical representation of the thermodynamic properties of substances by means of surfaces. *Trans. Connect. Acad.* **II December**, 382–404 (1873).
  48. Gibbs, J. W. Abstract of ‘the equilibrium of heterogeneous substances’. *Am. J. Sci.* **s3-16, Dec**, 441–458 (1878).
  49. Liu, Z. K. & Wang, Y. *Computational Thermodynamics of Materials*. (Cambridge University Press, 2016). doi:10.1017/CBO9781139018265
  50. Liu, Z. K. First-Principles calculations and CALPHAD modeling of thermodynamics. *J. Phase Equilibria Diffus.* **30**, 517–534 (2009).
  51. Born, M. & Oppenheimer, R. Quantum theory of molecules. *Ann. Phys.* **84**, 457–484 (1927).
  52. Ceperley, D. M. & Alder, B. J. Ground state of the electron gas by a stochastic method. *Phys. Rev. Lett.* **45**, 566–569 (1980).
  53. Perdew, J. P. & Zunger, A. Self-interaction correction to density-functional approximations for many-electron systems. *Phys. Rev. B* **23**, 5048–5079 (1981).
  54. Kresse, G. & Joubert, D. From ultrasoft pseudopotentials to the projector augmented-wave method. *Phys. Rev. B* **59**, 1758–1775 (1999).
  55. Shang, S.-L., Wang, Y., Kim, D. & Liu, Z.-K. First-principles thermodynamics from phonon and Debye model: Application to Ni and Ni<sub>3</sub>Al. *Comput. Mater. Sci.* **47**, 1040–1048 (2010).
  56. Wang, Y., Liao, M., Bocklund, B. J., Gao, P., Shang, S.-L., Kim, H., Beese, A. M., Chen, L.-Q. & Liu, Z.-K. DFTTK: Density Functional Theory ToolKit for high-throughput lattice dynamics calculations. *CALPHAD* **75**, 102355 (2021).
  57. DFTTK: Density Functional Theory Tool Kits. <https://www.dfttk.org/>
  58. Wang, Y., Shang, S., Liu, Z.-K. & Chen, L.-Q. Mixed-space approach for calculation of

- vibration-induced dipole-dipole interactions. *Phys. Rev. B* **85**, 224303 (2012).
59. Wang, Y., Chen, L.-Q. & Liu, Z.-K. YPHON: A package for calculating phonons of polar materials. *Comput. Phys. Commun.* **185**, 2950–2968 (2014).
  60. Wang, Y., Zhang, L. A., Shang, S. L., Liu, Z. K. & Chen, L. Q. Accurate calculations of phonon dispersion in CaF<sub>2</sub> and CeO<sub>2</sub>. *Phys. Rev. B* **88**, 24304 (2013).
  61. Liu, Z. K., Wang, Y. & Shang, S. Thermal Expansion Anomaly Regulated by Entropy. *Sci. Rep.* **4**, 7043 (2014).
  62. Coleman, B. D. & Truesdell, C. On the reciprocal relations of Onsager. *J. Chem. Phys.* **33**, 28–31 (1960).
  63. Truesdell, C. Mechanical basis of diffusion. *J. Chem. Phys.* **37**, 2336–2344 (1962).
  64. Andersson, J. & Ågren, J. Models for numerical treatment of multicomponent diffusion in simple phases. *J. Appl. Phys.* **72**, 1350–1355 (1992).
  65. de Groot, S. R. & Mazur, P. *Non-equilibrium thermodynamics*. (Dover Publications, Inc. New York, 1984).
  66. Kondepudi, D. & Prigogine, I. *Modern Thermodynamics: From Heat Engines to Dissipative Structures*. (John Wiley & Sons Ltd., 2015).
  67. Jou, D., Casas-Vázquez, J. & Lebon, G. *Extended irreversible thermodynamics*. (Springer Netherlands, 2010). doi:10.1007/978-90-481-3074-0
  68. Lebon, G. & Jou, D. Early history of extended irreversible thermodynamics (1953-1983): An exploration beyond local equilibrium and classical transport theory. *Eur. Phys. J. H* **40**, 205–240 (2015).
  69. Ågren, J. Computer simulations of diffusional reactions in multicomponent alloys with special applications to steel. PhD Thesis (1981).
  70. Bothe, D. in *Parabolic Problems: The Herbert Amann Festschrift* (eds. Escher, J., Guidotti, P., Hieber, M., Mucha, P., Prüss, J. W., Shibata, Y., Simonett, G., Walker, C. & Zajackowski, W.) 81–93 (Springer Basel, 2011). doi:10.1007/978-3-0348-0075-4\_5
  71. Allie-Ebrahim, T., Zhu, Q., Bräuer, P., Moggridge, G. D. & D’Agostino, C. Maxwell–Stefan diffusion coefficient estimation for ternary systems: an ideal ternary alcohol system. *Phys. Chem. Chem. Phys.* **19**, 16071–16077 (2017).
  72. Thermo-Calc Databases. Available at: <https://www.thermocalc.com/products-services/databases/>.
  73. CompuTherm Software and Databases. Available at: <http://www.computherm.com/>.
  74. Kirkaldy, J. S. & Young, D. J. *Diffusion in the condensed state*. (Institute of Metals, 1987).
  75. Liu, Z.-K., Höglund, L., Jönsson, B. & Ågren, J. An experimental and theoretical study of cementite dissolution in an Fe-Cr-C alloy. *Metall. Trans. A* **22**, 1745–1752 (1991).
  76. Helander, T. & Ågren, J. Computer simulation of multicomponent diffusion in joints of dissimilar steels. *Metall. Mater. Trans. A* **28**, 303–308 (1997).
  77. Darken, L. S. Diffusion in metal accompanied by phase change. *Trans. Am. Inst. Min. Metall. Eng.* **150**, 157–169 (1942).
  78. Darken, L. S. Diffusion, mobility and their interrelation through free energy in binary metallic systems. *Trans. Am. Inst. Min. Metall. Eng.* **175**, 184–201 (1948).
  79. Darken, L. S. Diffusion of carbon in austenite with a discontinuity in composition. *Trans. Am. Inst. Min. Metall. Eng.* **180**, 430–438 (1949).
  80. Andersson, J.-O., Helander, T., Höglund, L., Shi, P. & Sundman, B. Thermo-Calc &

- DICTRA, computational tools for materials science. *CALPHAD* **26**, 273–312 (2002).
81. Hillert, M. A solid-solution model for inhomogeneous systems. *Acta Metall.* **9**, 525–535 (1961).
  82. Cahn, J. W. On spinodal decomposition in cubic crystals. *Acta Metall.* **10**, 179–183 (1962).
  83. Chen, L.-Q. Phase-field models for microstructure evolution. *Annu. Rev. Mater. Res.* **32**, 113–140 (2002).
  84. Krishna, R. Uphill diffusion in multicomponent mixtures. *Chem. Soc. Rev.* **44**, 2812–2836 (2015).
  85. Kirkendall, E., Thomassen, L. & Upthegrove, C. Rates of diffusion of copper and zinc in alpha brass. *Trans. Am. Inst. Min. Metall. Eng.* **133**, 186–203 (1939).
  86. Kirkendall, E. O. Diffusion of zinc in alpha brass. *Trans. Am. Inst. Min. Metall. Eng.* **147**, 104–109 (1942).
  87. Smigelskas, A. D. & Kirkendall, E. O. Zinc diffusion in alpha-brass. *Trans. Am. Inst. Min. Metall. Eng.* **171**, 130–142 (1947).
  88. Höglund, L. & Ågren, J. Analysis of the Kirkendall effect, marker migration and pore formation. *Acta Mater.* **49**, 1311–1317 (2001).
  89. Campbell, C. E., Zhao, J.-C. & Henry, M. F. Comparison of Experimental and Simulated Multicomponent Ni-Base Superalloy Diffusion Couples. *J. Phase Equilibria Diffus.* **25**, 6–15 (2004).
  90. Mantina, M., Wang, Y., Arroyave, R., Chen, L. Q., Liu, Z. K. & Wolverton, C. First-Principles Calculation of Self-Diffusion Coefficients. *Phys. Rev. Lett.* **100**, 215901 (2008).
  91. Mantina, M., Shang, S. L., Wang, Y., Chen, L. Q. & Liu, Z. K. 3 d transition metal impurities in aluminum: A first-principles study. *Phys. Rev. B* **80**, 184111 (2009).
  92. Mantina, M., Wang, Y., Chen, L. Q., Liu, Z. K. & Wolverton, C. First principles impurity diffusion coefficients. *Acta Mater.* **57**, 4102–4108 (2009).
  93. Hargather, C. Z., Shang, S.-L., Liu, Z.-K. & Du, Y. A first-principles study of self-diffusion coefficients of fcc Ni. *Comput. Mater. Sci.* **86**, 17–23 (2014).
  94. Hargather, C. Z., Shang, S. L. & Liu, Z. K. A comprehensive first-principles study of solute elements in dilute Ni alloys: Diffusion coefficients and their implications to tailor creep rate. *Acta Mater.* **157**, 126–141 (2018).
  95. Mantina, M., Chen, L. Q. & Liu, Z. K. Predicting Diffusion Coefficients from First-principles via Eyring’s Reaction Rate Theory. *Defect Diffus. Forum* **294**, 1–13 (2009).
  96. Ganeshan, S., Shang, S. L., Zhang, H., Wang, Y., Mantina, M. & Liu, Z. K. Elastic constants of binary Mg compounds from first-principles calculations. *Intermetallics* **17**, 313–318 (2009).
  97. Zhou, B.-C., Shang, S.-L., Wang, Y. & Liu, Z. K. Diffusion coefficients of alloying elements in dilute Mg alloys: A comprehensive first-principles study. *Acta Mater.* **103**, 573–586 (2016).
  98. Shang, S. L., Hector, L. G., Wang, Y. & Liu, Z. K. Anomalous energy pathway of vacancy migration and self-diffusion in hcp Ti. *Phys. Rev. B* **83**, 224104 (2011).
  99. Eyring, H. The Activated Complex in Chemical Reactions. *J. Chem. Phys.* **3**, 107–115 (1935).
  100. Vineyard, G. H. Frequency factors and isotope effects in solid state rate processes. *J. Phys. Chem. Solids* **3**, 121–127 (1957).



101. Henkelman, G., Uberuaga, B. P. & Jónsson, H. A climbing image nudged elastic band method for finding saddle points and minimum energy paths. *J. Chem. Phys.* **113**, 9901–9904 (2000).
102. Le Claire, A. D. Solute diffusion in dilute alloys. *J. Nucl. Mater.* **69–70**, 70–96 (1978).
103. Wimmer, E., Wolf, W., Sticht, J., Saxe, P., Geller, C. B., Najafabadi, R. & Young, G. A. Temperature-dependent diffusion coefficients from ab initio computations: Hydrogen, deuterium, and tritium in nickel. *Phys. Rev. B* **77**, 134305 (2008).
104. Höglund, L. & Ågren, J. Simulation of Carbon Diffusion in Steel Driven by a Temperature Gradient. *J. Phase Equilibria Diffus.* **31**, 212–215 (2010).
105. Krajewski, A. M., Siegel, J. W., Xu, J. & Liu, Z. K. Extensible Structure-Informed Prediction of Formation Energy with improved accuracy and usability employing neural networks. *Comput. Mater. Sci.* **208**, 111254 (2022).
106. Li, K., DeCost, B., Choudhary, K., Greenwood, M. & Hattrick-Simpers, J. A critical examination of robustness and generalizability of machine learning prediction of materials properties. *npj Comput. Mater.* **9**, 55 (2023).
107. Fultz, B. Vibrational thermodynamics of materials. *Prog. Mater. Sci.* **55**, 247–352 (2010).
108. Guillaume, C. E. Recherches sur les aciers au nickel. Dilatations aux températures elevees; resistance électrique. *C. R. Acad. Sci. Paris* **125**, 235–238 (1897).
109. GUILLAUME, C.-E. Invar. *Nature* **131**, 658–658 (1933).
110. Wittenauer, J. *The Invar effect: A centennial symposium: An International Symposium on the Invar Effect held on the occasion of the 100th anniversary of its discovery* (The Minerals, Metals & Materials Society (TMS), 1997).
111. Shang, S., Zhang, H., Ganeshan, S. & Liu, Z.-K. The development and application of a thermodynamic database for magnesium alloys. *JOM* **60**, 45–47 (2008).
112. Zhang, H., Wang, Y., Shang, S., Chen, L.-Q. & Liu, Z.-K. Thermodynamic modeling of Mg–Ca–Ce system by combining first-principles and CALPHAD method. *J. Alloys Compd.* **463**, 294–301 (2008).
113. Liu, Z.-K., Wang, Y. & Shang, S.-L. Origin of negative thermal expansion phenomenon in solids. *Scr. Mater.* **65**, 664–667 (2011).
114. Shang, S.-L., Wang, Y. & Liu, Z. K. Quantifying the degree of disorder and associated phenomena in materials through zentropy: Illustrated with Invar Fe<sub>3</sub>Pt. *Scr. Mater.* **225**, 115164 (2023).
115. Shang, S.-L., Wang, Y. & Liu, Z.-K. Thermodynamic fluctuations between magnetic states from first-principles phonon calculations: The case of bcc Fe. *Phys. Rev. B* **82**, 014425 (2010).
116. Shang, S. L., Saal, J. E., Mei, Z. G., Wang, Y. & Liu, Z. K. Magnetic thermodynamics of fcc Ni from first-principles partition function approach. *J. Appl. Phys.* **108**, 123514 (2010).
117. Wang, Y., Shang, S. L., Hui, X. D., Chen, L. Q. & Liu, Z. K. Effects of spin structures on phonons in BaFe<sub>2</sub>As<sub>2</sub>. *Appl. Phys. Lett.* **97**, 022504 (2010).
118. Wang, Y., Saal, J. E., Shang, S. L., Hui, X. D., Chen, L. Q. & Liu, Z. K. Effects of spin structures on Fermi surface topologies in BaFe<sub>2</sub>As<sub>2</sub>. *Solid State Commun.* **151**, 272–275 (2011).
119. Wang, Y., Shang, S. L., Chen, L. Q. & Liu, Z. K. Magnetic excitation and thermodynamics of BaFe<sub>2</sub>As<sub>2</sub>. *Int. J. Quantum Chem.* **111**, 3565–3570 (2011).

120. Liu, Z. K., Shang, S.-L., Du, J. & Wang, Y. Parameter-free prediction of phase transition in PbTiO<sub>3</sub> through combination of quantum mechanics and statistical mechanics. *Scr. Mater.* **232**, 115480 (2023).
121. Krisch, M., Farber, D. L., Xu, R., Antonangeli, D., Aracne, C. M., Beraud, A., Chiang, T. C., Zarestky, J., Kim, D. Y., Isaev, E. I., Ahuja, R. & Johansson, B. Phonons of the anomalous element cerium. *Proc. Natl. Acad. Sci.* **108**, 9342–9345 (2011).
122. Liu, Z.-K., Hew, N. L. E. & Shang, S.-L. Zentropy theory for accurate prediction of free energy, volume, and thermal expansion without fitting parameters. *Microstructures* **4**, 2024009 (2024).
123. Liu, Z.-K. DE-SC0023185: Zentropy Theory for Transformative Functionalities of Magnetic and Superconducting Materials. Available at: <https://pamspublic.science.energy.gov/WebPAMSEExternal/Interface/Common/ViewPublicAbstract.aspx?rv=abfd1695-37b7-463d-9046-6eff5ac326e3&rtc=24&PRoleId=10>.
124. Lau, B. & Millis, A. J. Theory of the Magnetic and Metal-Insulator Transitions in RNiO<sub>3</sub> Bulk and Layered Structures. *Phys. Rev. Lett.* **110**, 126404 (2013).
125. Middey, S., Chakhalian, J., Mahadevan, P., Freeland, J. W., Millis, A. J. & Sarma, D. D. Physics of Ultrathin Films and Heterostructures of Rare-Earth Nickelates. *Annu. Rev. Mater. Res.* **46**, 305–334 (2016).
126. Zunger, A., Wei, S. H., Ferreira, L. G. & Bernard, J. E. Special Quasirandom Structures. *Phys. Rev. Lett.* **65**, 353–356 (1990).
127. Jiang, C., Wolverton, C., Sofo, J., Chen, L. Q. & Liu, Z. K. First-principles study of binary bcc alloys using special quasirandom structures. *Phys. Rev. B* **69**, 214202 (2004).
128. Evans, D. J., Cohen, E. G. D. & Morriss, G. P. Probability of second law violations in shearing steady states. *Phys. Rev. Lett.* **71**, 2401–2404 (1993).
129. Jarzynski, C. Nonequilibrium Equality for Free Energy Differences. *Phys. Rev. Lett.* **78**, 2690–2693 (1997).
130. Wang, G. M., Sevick, E. M., Mittag, E., Searles, D. J. & Evans, D. J. Experimental Demonstration of Violations of the Second Law of Thermodynamics for Small Systems and Short Time Scales. *Phys. Rev. Lett.* **89**, 050601 (2002).
131. Jarzynski, C. Equalities and Inequalities: Irreversibility and the Second Law of Thermodynamics at the Nanoscale. *Annu. Rev. Condens. Matter Phys.* **2**, 329–351 (2011).
132. Sagawa, T. & Ueda, M. Fluctuation Theorem with Information Exchange: Role of Correlations in Stochastic Thermodynamics. *Phys. Rev. Lett.* **109**, 180602 (2012).
133. Maillet, O., Erdman, P. A., Cavina, V., Bhandari, B., Mannila, E. T., Peltonen, J. T., Mari, A., Taddei, F., Jarzynski, C., Giovannetti, V. & Pekola, J. P. Optimal Probabilistic Work Extraction beyond the Free Energy Difference with a Single-Electron Device. *Phys. Rev. Lett.* **122**, 150604 (2019).
134. Seifert, U. Entropy and the second law for driven, or quenched, thermally isolated systems. *Phys. A* **552**, 121822 (2020).
135. Bird and Cage Thaumatrope. Available at: <https://youtu.be/46Mlr4hvW-E>. (Accessed: 4th February 2024)
136. Sicron, N., Ravel, B., Yacoby, Y., Stern, E. A., Dogan, F. & Rehr, J. J. Nature of the ferroelectric phase transition in PbTiO<sub>3</sub>. *Phys. Rev. B* **50**, 13168–13180 (1994).
137. Sicron, N., Ravel, B., Yacoby, Y., Stern, E. A., Dogan, F. & Rehr, J. J. The ferroelectric phase transition in PbTiO<sub>3</sub> from a local perspective. *Phys. B* **208–209**, 319–320 (1995).

138. Ravel, B., Sicron, N., Yacoby, Y., Stern, E. A., Dogan, F., Rehr, J. J., Slcron, N., Yacoby, Y., Stern, E. A., Dogan, F. & Rehr, J. J. Order-disorder behavior in the phase transition of PbTiO<sub>3</sub>. *Ferroelectrics* **164**, 265–277 (1995).
139. Fang, H., Wang, Y., Shang, S. & Liu, Z. K. Nature of ferroelectric-paraelectric phase transition and origin of negative thermal expansion in PbTiO<sub>3</sub>. *Phys. Rev. B* **91**, 024104 (2015).
140. Shirane, G. & Hoshino, S. On the phase transition in lead titanate. *J. Phys. Soc. Japan* **6**, 265–270 (1951).
141. Wang, Y., Hu, Y.-J., Bocklund, B., Shang, S.-L., Zhou, B.-C., Liu, Z. K. & Chen, L.-Q. First-principles thermodynamic theory of Seebeck coefficients. *Phys. Rev. B* **98**, 224101 (2018).
142. Wang, Y., Chong, X., Hu, Y. J., Shang, S. L., Drymiotis, F. R., Firdosy, S. A., Star, K. E., Fleurial, J. P., Ravi, V. A., Chen, L. Q. & Liu, Z. K. An alternative approach to predict Seebeck coefficients: Application to La<sub>3-x</sub>Te<sub>4</sub>. *Scr. Mater.* **169**, 87–91 (2019).
143. Iacopini, S. & Piazza, R. Thermophoresis in protein solutions. *Europhys. Lett.* **63**, 247–253 (2003).
144. Kita, R., Polyakov, P. & Wiegand, S. Ludwig–Soret Effect of Poly( N - isopropylacrylamide): Temperature Dependence Study in Monohydric Alcohols. *Macromolecules* **40**, 1638–1642 (2007).
145. Kishikawa, Y., Wiegand, S. & Kita, R. Temperature Dependence of Soret Coefficient in Aqueous and Nonaqueous Solutions of Pullulan. *Biomacromolecules* **11**, 740–747 (2010).
146. Iacopini, S., Rusconi, R. & Piazza, R. The “macromolecular tourist”: Universal temperature dependence of thermal diffusion in aqueous colloidal suspensions. *Eur. Phys. J. E* **19**, 59–67 (2006).
147. de Gans, B.-J., Kita, R., Wiegand, S. & Luettmmer-Strathmann, J. Unusual Thermal Diffusion in Polymer Solutions. *Phys. Rev. Lett.* **91**, 245501 (2003).
148. Costesèque, P. & Loubet, J.-C. Measuring the Soret coefficient of binary hydrocarbon mixtures in packed thermogravitational columns (contribution of Toulouse University to the benchmark test). *Philos. Mag.* **83**, 2017–2022 (2003).
149. Hartmann, S., Wittko, G., Köhler, W., Morozov, K. I., Albers, K. & Sadowski, G. Thermophobicity of Liquids: Heats of Transport in Mixtures as Pure Component Properties. *Phys. Rev. Lett.* **109**, 065901 (2012).
150. Schraml, M., Bataller, H., Bauer, C., Bou-Ali, M. M., Croccolo, F., Lapeira, E., Mialdun, A., Möckel, P., Ndjaka, A. T., Shevtsova, V. & Köhler, W. The Soret coefficients of the ternary system water/ethanol/triethylene glycol and its corresponding binary mixtures. *Eur. Phys. J. E* **44**, 128 (2021).
151. Rahman, M. A. & Saghir, M. Z. Thermodiffusion or Soret effect: Historical review. *Int. J. Heat Mass Transf.* **73**, 693–705 (2014).
152. Tu, K. N. Recent advances on electromigration in very-large-scale-integration of interconnects. *J. Appl. Phys.* **94**, 5451 (2003).
153. Chen, C., Tong, H. M. & Tu, K. N. Electromigration and Thermomigration in Pb-Free Flip-Chip Solder Joints. *Annu. Rev. Mater. Res.* **40**, 531–555 (2010).
154. Tu, K. N., Liu, Y. & Li, M. Effect of Joule heating and current crowding on electromigration in mobile technology. *Appl. Phys. Rev.* **4**, 011101 (2017).
155. Tu, K. N. & Gusak, A. N. Mean-Time-To-Failure Equations for Electromigration,

- Thermomigration, and Stress Migration. *IEEE Trans. Components, Packag. Manuf. Technol.* **10**, 1427–1431 (2020).
156. Kirchheim, R. Stress and electromigration in Al-lines of integrated circuits. *Acta Metall. Mater.* **40**, 309–323 (1992).
  157. Basaran, C., Lin, M. & Ye, H. A thermodynamic model for electrical current induced damage. *Int. J. Solids Struct.* **40**, 7315–7327 (2003).
  158. Wiseman, G. G. & Kuebler, J. K. Electrocaloric Effect in Ferroelectric Rochelle Salt. *Phys. Rev.* **131**, 2023–2027 (1963).
  159. Lombardo, G. & Pohl, R. O. Electrocaloric Effect and a New Type of Impurity Mode. *Phys. Rev. Lett.* **15**, 291–293 (1965).
  160. Lu, S.-G. & Zhang, Q. Electrocaloric Materials for Solid-State Refrigeration. *Adv. Mater.* **21**, 1983–1987 (2009).
  161. Scott, J. F. Electrocaloric Materials. *Annu. Rev. Mater. Res.* **41**, 229–240 (2011).
  162. Moya, X., Kar-Narayan, S. & Mathur, N. D. Caloric materials near ferroic phase transitions. *Nat. Mater.* **13**, 439–450 (2014).
  163. Moya, X. & Mathur, N. D. Caloric materials for cooling and heating. *Science* **370**, 797–803 (2020).
  164. Qian, X., Han, D., Zheng, L., Chen, J., Tyagi, M., Li, Q., Du, F., Zheng, S., Huang, X., Zhang, S., Shi, J., Huang, H., Shi, X., Chen, J., Qin, H., Bernholc, J., Chen, X., Chen, L.-Q., Hong, L. & Zhang, Q. M. High-entropy polymer produces a giant electrocaloric effect at low fields. *Nature* **600**, 664–669 (2021).
  165. Caspari, M. E. & Merz, W. J. The Electromechanical Behavior of BaTiO<sub>3</sub> Single-Domain Crystals. *Phys. Rev.* **80**, 1082–1089 (1950).
  166. Kulcsar, F. Electromechanical Properties of Lead Titanate Zirconate Ceramics Modified with Certain Three-or Five-Valent Additions. *J. Am. Ceram. Soc.* **42**, 343–349 (1959).
  167. Somlyo, A. V & Somlyo, A. P. Electromechanical and pharmacomechanical coupling in vascular smooth muscle. *J. Pharmacol. Exp. Ther.* **159**, 129–45 (1968).
  168. Zhao, J., Zhang, Q. M., Kim, N. & Shrout, T. Electromechanical Properties of Relaxor Ferroelectric Lead Magnesium Niobate-Lead Titanate Ceramics. *Jpn. J. Appl. Phys.* **34**, 5658–5663 (1995).
  169. Park, S.-E. & Shrout, T. R. Ultrahigh strain and piezoelectric behavior in relaxor based ferroelectric single crystals. *J. Appl. Phys.* **82**, 1804–1811 (1997).
  170. Fu, H. & Cohen, R. E. Polarization rotation mechanism for ultrahigh electromechanical response in single-crystal piezoelectrics. *Nature* **403**, 281–283 (2000).
  171. Kutnjak, Z., Petzelt, J. & Blinc, R. The giant electromechanical response in ferroelectric relaxors as a critical phenomenon. *Nature* **441**, 956–959 (2006).
  172. Ahart, M., Somayazulu, M., Cohen, R. E., Ganesh, P., Dera, P., Mao, H., Hemley, R. J., Ren, Y., Liermann, P. & Wu, Z. Origin of morphotropic phase boundaries in ferroelectrics. *Nature* **451**, 545–548 (2008).
  173. Li, F., Cabral, M. J., Xu, B., Cheng, Z., Dickey, E. C., LeBeau, J. M., Wang, J., Luo, J., Taylor, S., Hackenberger, W., Bellaiche, L., Xu, Z., Chen, L.-Q., Shrout, T. R. & Zhang, S. Giant piezoelectricity of Sm-doped Pb(Mg 1/3 Nb 2/3 )O 3 -PbTiO 3 single crystals. *Science* **364**, 264–268 (2019).

Table 1: Physical quantities related to 1<sup>st</sup> directives between molar quantities (first column) and potentials (first row), slightly modified from Ref. <sup>33</sup>.

	$T$ , Temperature	$\sigma$ , Stress	$E$ , Electrical field	$\mathcal{H}$ , Magnetic field	$\mu_i$ , Chemical potential
$S$ , Entropy	Heat capacity	Piezocaloric effect	Electrocaloric effect	Magnetocaloric effect	$\frac{\partial S}{\partial \mu_k}$
$\epsilon$ , Strain	Thermal expansion	Elastic compliance	Converse piezoelectricity	Piezomagnetic moduli	$\frac{\partial \epsilon_{ij}}{\partial \mu_k}$
$\theta$ , Electric displacement	Pyroelectric coefficients	Piezoelectric moduli	Permittivity	Magnetolectric coefficient	$\frac{\partial D_i}{\partial \mu_k}$
$B$ , Magnetic induction	Pyromagnetic coefficient	Piezomagnetic moduli	Electromagnetic coefficient	Permeability	$\frac{\partial B_i}{\partial \mu_k}$
$N_j$ , Moles	<i>Thermoreactivity</i>	<i>Stressoreactivity</i>	<i>Electroreactivity</i>	<i>Magnetoreactivity</i>	$\frac{\partial N_i}{\partial \mu_k}$ , <i>Thermodynamic factor</i>

Table 2: Cross phenomenon coefficients represented by 1st derivatives between potentials, slightly modified from Ref. <sup>33</sup>.

	$T$ , Temperature	$\sigma$ , Stress	$E$ , Electrical field	$\mathcal{H}$ , Magnetic field	$\mu_i$ , Chemical potential
$T$	1	$-\frac{\partial S}{\partial \epsilon}$	$-\frac{\partial S}{\partial \theta}$	$-\frac{\partial S}{\partial B}$	$-\frac{\partial S}{\partial c_i}$ Partial entropy
$\sigma$	$\frac{\partial \sigma}{\partial T}$ , Thermostress	1	$-\frac{\partial \epsilon}{\partial \theta}$	$-\frac{\partial \epsilon}{\partial B}$	$-\frac{\partial \epsilon}{\partial c_i}$ Partial strain
$E$	$\frac{\partial E}{\partial T}$ , Thermoelectric	$\frac{\partial E}{\partial \sigma}$ , Piezoelectric	1	$-\frac{\partial \theta}{\partial B}$	$-\frac{\partial \theta}{\partial c_i}$ Partial electrical displacement
$\mathcal{H}$	$\frac{\partial \mathcal{H}}{\partial T}$ , Thermomagnetic	$\frac{\partial \mathcal{H}}{\partial \sigma}$ , Piezomagnetic	$\frac{\partial \mathcal{H}}{\partial E}$ , Electromagnetic	1	$-\frac{\partial B}{\partial c_i}$ Partial magnetic induction
$\mu_i$	$\frac{\partial \mu_i}{\partial T}$ , Thermodiffusion	$\frac{\partial \mu_i}{\partial \sigma}$ , Stressmigration	$\frac{\partial \mu_i}{\partial E}$ , Electromigration	$\frac{\partial \mu_i}{\partial \mathcal{H}}$ , Magnetomigration	$\frac{\partial \mu_i}{\partial \mu_j} = -\frac{\partial c_j}{\partial c_i} = \frac{\Phi_{ij}}{\Phi_{ji}}$ Crossdiffusion

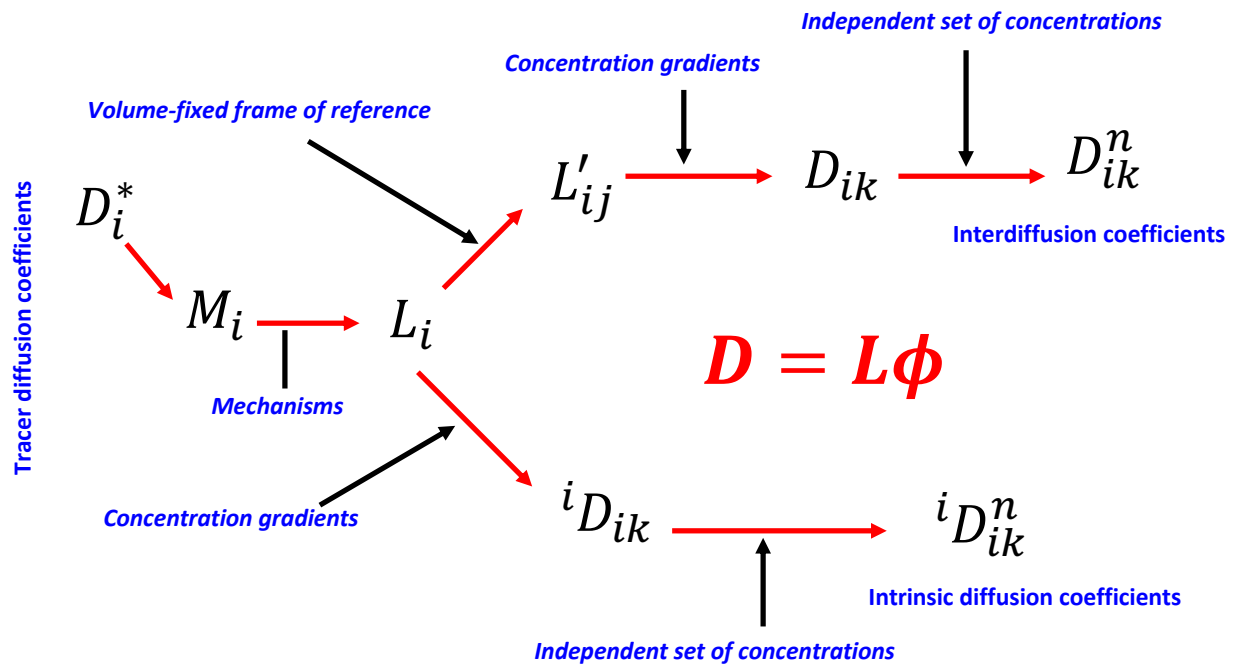
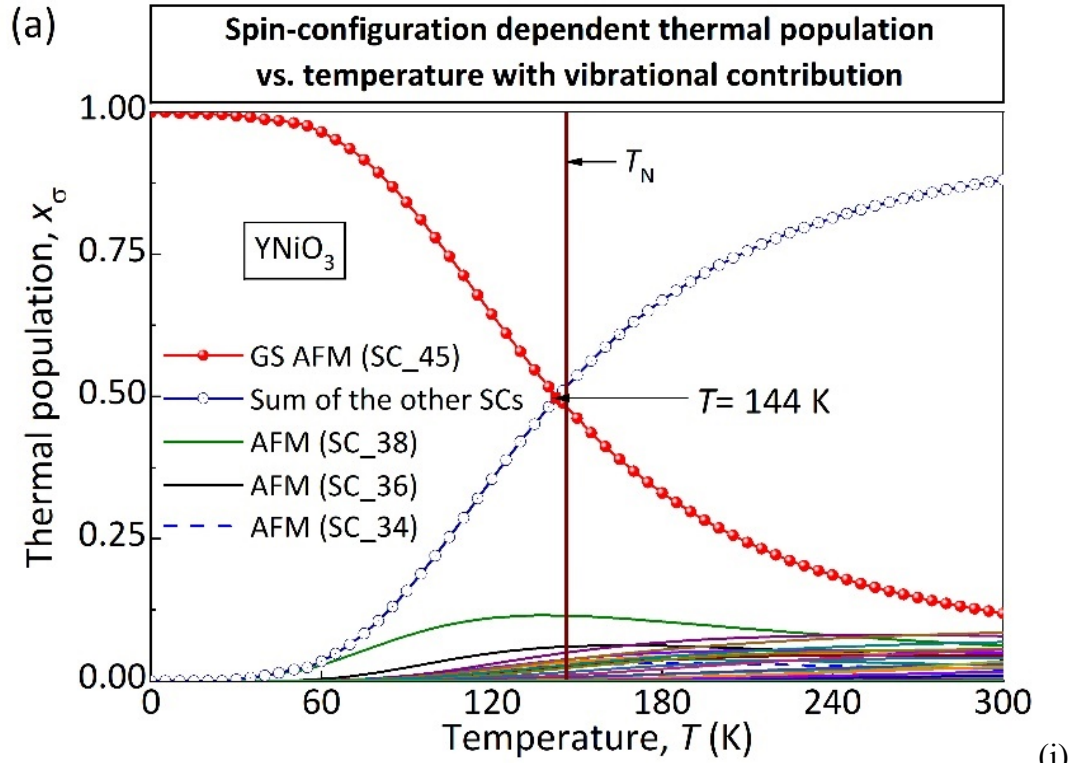
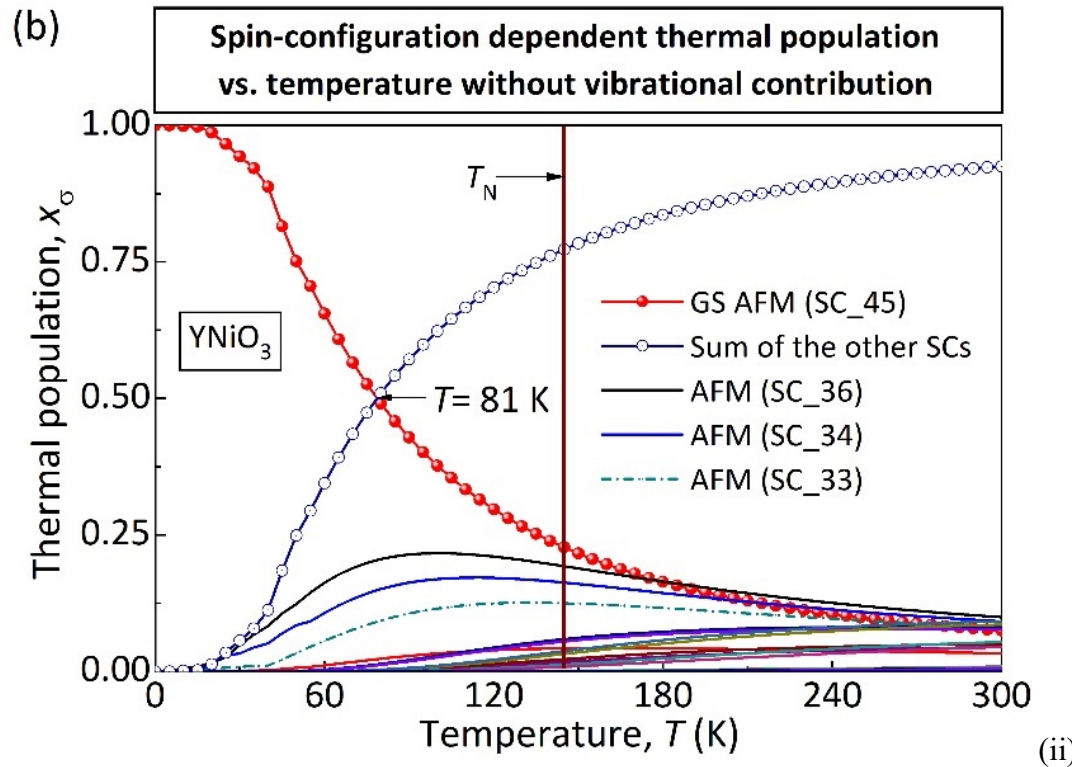


Figure 1



(i)



(ii)



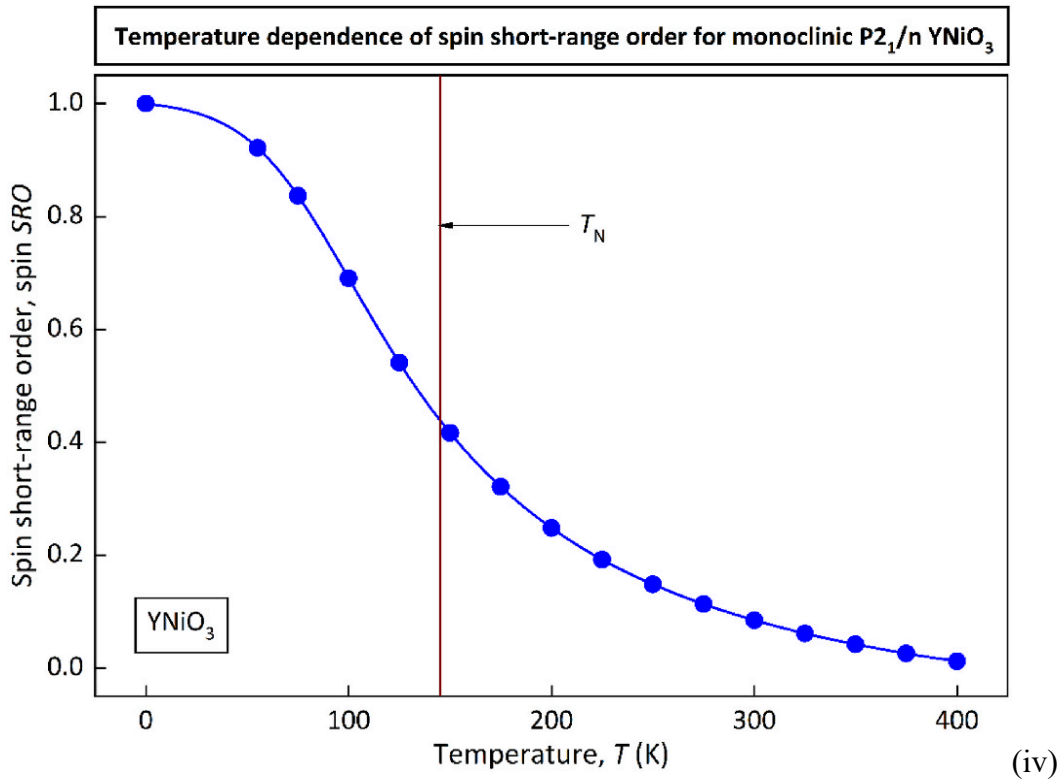
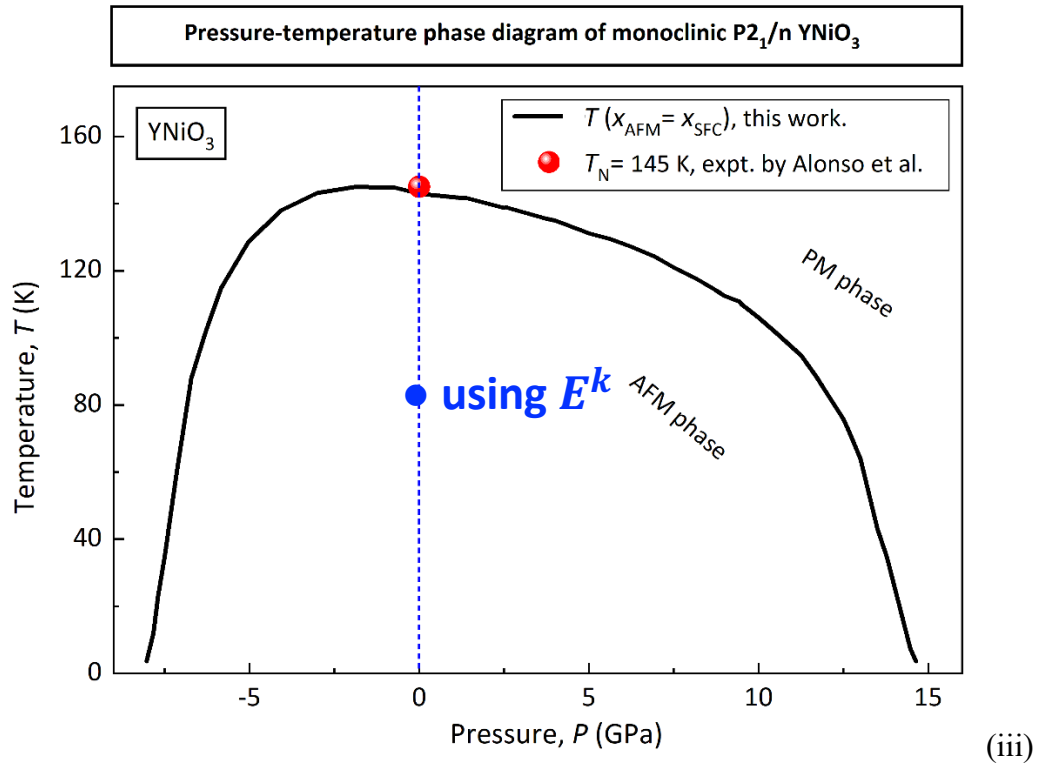


Figure 2